NASA TN D-187

TECHNICAL NOTE

D-187

EXPERIMENTAL INVESTIGATION OF ASPECT-RATIO-1 SUPERCAVITATING HYDROFOILS AT SPEEDS UP TO 185 FEET PER SECOND

By Kenneth W. Christopher and Virgil E. Johnson, Jr.

Langley Research Center
Langley Field, Va.

NATIONAL AERONAUTICS AND SPACE ADMINISTRATION

WASHINGTON

January 1960

1A

NATIONAL AERONAUTICS AND SPACE ADMINISTRATION

TECHNICAL NOTE D-187

EXPERIMENTAL INVESTIGATION OF ASPECT-RATIO-1 SUPERCAVITATING HYDROFOILS AT SPEEDS UP TO 185 FEET PER SECOND

By Kenneth W. Christopher and Virgil E. Johnson, Jr.

SUMMARY

An experimental investigation has been made in the Langley high-speed hydrodynamics facility to determine the force and moment characteristics of two aspect-ratio-1 supercavitating hydrofoils (one having a flat bottom and one having camber) operating at zero cavitation number. Measurements were made of lift, drag, pitching moment, and spray location over a range of angles of attack from 3° to 20° for depths varying from 0 to approximately 1 chord. Tests were also made with the flat-bottomed hydrofoil at finite cavitation numbers to extend the range of data down to a cavitation number of 0.07. The range of speeds for the investigation was from 60 to 185 feet per second.

The results of the zero-cavitation-number tests are in good agreement with theoretical values of forces and moments. Experimental values of spray location are not in agreement with theory at high angles of attack but the agreement improves with decreasing angle of attack and the theory gives a good indication of the minimum angle of attack for which the two hydrofoils can be operated with a cavity from the leading edge.

INTRODUCTION

Hydrofoils of conventional airfoil section have not proved to be satisfactory for use as auxiliary lifting surfaces for high-speed boats or seaplanes because of certain operating problems. As the hydrofoil approaches the free-water surface, the low-pressure side of the hydrofoil becomes ventilated from the atmosphere, resulting in a severe and abrupt loss in lift. If the hydrofoil is operated at a depth great enough to prevent ventilation, the pressure on the upper surface of the hydrofoil will continue to decrease with increase in speed until vapor pressure is reached and a cavity forms in the flow over the upper surface of the hydrofoil. This phenomenon, which occurs at speeds less

than the takeoff speeds of current high-speed aircraft, is also accompanied by loss in lift and lift-drag ratio (refs. 1 and 2).

A family of hydrofoil sections has been derived (ref. 3) that will operate in the cavitated or ventilated condition with characteristics superior to conventional airfoil sections operating under similar conditions. One hydrofoil of that family is described in reference 4 together with the results from an experimental investigation made with that hydrofoil and a flat-bottomed hydrofoil in Langley tank no. 2. The range of depths covered for ventilated or zero-cavitation-number tests was limited by speed limitations on the carriage and by the type of strut used. The maximum carriage speed also determined the minimum nonzero or finite cavitation number at which the hydrofoil could be tested.

The purpose of the present zero-cavitation-number tests was to obtain force and moment data and values of minimum angle of attack of the hydrofoils at depths of submersion up to 1 chord for comparison with the theory presented in reference 4. The finite-cavitation-number tests were made to extend the range of available data for the flat-bottomed hydrofoil to lower cavitation numbers for comparison with values predicted by the method given by Wu in reference 5 and by others.

SYMBOLS

C_L lift coefficient, $\frac{\text{Lift}}{qS}$

$C_{L,\sigma}$ lift coefficient at finite cavitation number

C_D drag coefficient, $\frac{\text{Drag}}{qS}$

$C_{m,c/4}$ moment coefficient about quarter chord, $\frac{\text{Moment}}{qSc}$

C_{cp} center-of-pressure coefficient, $\frac{\text{Distance from leading edge}}{\text{Chord}}$

c chord length, ft

d/c depth of submersion with respect to chord, measured from local mean water surface to leading edge

h height of spray above reference line, measured perpendicular to reference line

h_p distance from upper cavity streamline to reference line along path of probe

L/D lift-drag ratio

l wetted length on upper surface of hydrofoil

p local pressure on hydrofoil, lb/sq ft

p_o free-stream pressure at mean depth of hydrofoil, lb/sq ft

p_c cavity pressure, lb/sq ft

p_v vapor pressure, lb/sq ft

q dynamic pressure, $\frac{\rho V^2}{2}$

S hydrofoil area, sq ft

V speed, fps

x,y coordinates

α angle of attack, deg

δ/c spray thickness with respect to chord

ρ mass density of water, $\frac{\text{slugs}}{\text{cu ft}}$

σ cavitation number, $\frac{p_o - p}{q}$

σ_c cavitation number based on cavity pressure, $\frac{p_o - p_c}{q}$

σ_v cavitation number based on vapor pressure, $\frac{p_o - p_v}{q}$

Subscripts:

l lower surface

u upper surface

1,2 speed conditions

DESCRIPTION OF MODELS

The models used for the present investigation were two aspect-ratio-1 hydrofoils that had been used previously for the tests reported in reference 4. A photograph of the cambered and flat-bottomed hydrofoils and the parabolic strut is shown in figure 1. A drawing of the flat-bottomed hydrofoil mounted on the streamlined and the parabolic struts is shown in figure 2. A sketch of the profile of the cambered hydrofoil and a table of coordinates are presented in figure 3. Both hydrofoils had a 7.071-inch chord and had sharp leading and trailing edges. The flat-bottomed hydrofoil had a triangular cross section 5 percent thick at midchord. The cambered hydrofoil had a Tulin-Burkart section (ref. 3) with a design lift coefficient of 0.392. The forward half-chord of the top surface of the cambered model was designed (by using two-dimensional flat-plate theory) to conform with the under surface of the spray jet leaving the leading edge as computed for an angle of attack of 5°.

A strut having an NACA 66_1-012 section was used for the finite-cavitation-number tests. A small opening near the bottom of the strut led to a passage inside the strut so that pressures in the cavity over the hydrofoil could be measured. A blunt-trailing-edge strut (parabolic section) was used for the zero-cavitation-number tests to provide a passageway for venting the top surface of the hydrofoil to the atmosphere and thus to simulate the zero-cavitation-number condition. The parabolic section was used because it produces minimum drag in cavity flow. For a limited number of runs, a 1/4-inch brass tube was soldered to the rear of the parabolic strut and was used for measuring the cavity pressures (fig. 2).

APPARATUS AND PROCEDURE

The investigation was conducted at the Langley high-speed hydrodynamics facility and utilized the temporary boom on the landing-loads carriage. The facility and its operation are described in reference 6. A photograph of the test setup is shown in figure 4.

Lift, drag, and pitching moments were measured over a range of speeds from 72 to 185 feet per second by an electrical strain-gage balance attached to a hydraulically operated towing staff that could be raised or lowered to provide changes in depth of submersion of the model. The depth of submersion was measured from the local mean water surface to the leading edge of the model. The angle of attack was corrected for structural deflections on the basis of calibrations made prior to the tests. A small number of finite-cavitation-number runs

were made in the Langley tank no. 2 to provide supplementary data between the range obtainable at the high-speed facility and that presented in reference 4.

The outputs of the strain-gage balance were supplied to strip-chart recorders located on the carriage. Force, moment, water-level, and strut-rise measurements were continuously recorded and coordinated at the three photographic stations (located approximately 555 feet, 1,030 feet, and 1,510 feet from the start of the run) at which readings were taken. Photographs of the model were taken from above and below the water surface at the same stations. High-speed flash lamps located one on each side of the underwater cameras were used for lighting. A sketch of the longitudinal and transverse sections of the tank at a photographic station is shown in figure 5.

Data were obtained at three depths of submersion on most of the zero-cavitation-number runs by allowing the towing staff to rise slowly during the run. The towing staff started to rise with the opening of a valve in the hydraulic line to the towing staff. A rope, with one end wrapped around a drum attached to the valve and the other end attached to a post on the ground, caused the valve to open as the carriage started to move. A slide-wire, the output of which was supplied to an oscillograph on the carriage, was used for recording the rise of the towing staff.

The thickness and the vertical location of the jet of spray from the leading edge of the hydrofoil were measured by using a probe mechanism (fig. 4). The probe blade had a parabolic cross section and enclosed a small tube that protruded through an opening at the tip. The tube was connected to a pressure cell on the strut supporting the blade. Before each run, the probe was adjusted so that the tip, at the bottom of the stroke, was located 1/4 inch vertically above the midchord position measured along the top of the hydrofoil. The blade was cycled down and up by an air-operated piston through a stroke of 8 inches at each of the recording stations. The system was triggered by a magnet at each of the recording stations. A circular slide-wire, geared to the piston, was used for measuring probe displacement. The outputs of the pressure cell and the slide-wire were recorded by the oscillograph on the carriage.

The mean water level at each recording station was measured by means of a float-type instrument. The float (a hollow, bronze cylinder 1 inch in diameter and 6 inches long) was attached to the side of the tank at a fixed height approximately one-half submerged with its axis perpendicular to the water surface. The buoyant force on the cylinder, which varied with the water level, was measured by a strain-gage pickup and recorded by an oscillograph. The character of the instrument was such that it did not respond to small waves.

The procedure followed for the finite-cavitation-number tests was the same as that for the zero-cavitation-number tests except that the probe was not used and the hydrofoil was set to run at a constant depth.

SCOPE AND ACCURACY

The finite-cavitation-number tests were made at a nominal constant depth of 6 inches over a range of speeds from 60 to 164 feet per second resulting in cavitation numbers (based on cavity pressure) of 0.533 to 0.076.

The zero-cavitation-number tests were made over a range of depths of submersion from 0 to 1 chord for angles of attack of 0° to 20°. Carriage speeds of 117 to 185 feet per second were recorded during these tests.

The accuracy of the quantities measured is estimated to be within the following limits:

Lift, lb	±25.0
Drag, lb	±15.0
Moment, ft-lb	±15.0
Angle of attack, deg	±0.10
Depth of submersion, in.	±0.10
Cavity pressure, lb/sq ft	±12.0
Spray thickness, in.	±0.02
Speed, fps	±0.15

The force and moment data were converted to coefficient form by using the density of the water measured during the tests (1.941 slugs per cubic foot). Because of the variation of temperature, the kinematic viscosity of the tank water varied from 0.93×10^{-5} to 1.52×10^{-5} square feet per second during the tests. The drag and moment data were corrected for the effect of the deceleration of the carriage and the drag data were also corrected for the strut drag. The strut water drag was calculated by using aerodynamic data for the streamlined strut and the form drag of a parabola for the parabolic strut; a coefficient increment of 0.003 for friction drag was added and any surface effects were neglected.

RESULTS AND DISCUSSION

The experimental data obtained in this investigation are presented in tables I to III.

Finite Cavitation Number

The results of the finite-cavitation-number tests made with the flat-bottomed hydrofoil mounted on the streamlined strut are presented in this section. Lift- and drag-coefficient data are plotted in figures 6(a) and (b). The present data and the supplementary data from Langley tank No. 2 are plotted against the cavitation number based on measured cavity pressure in figure 6(a). The same data are plotted against the cavitation number based on vapor pressure in figure 6(b) for comparison with data from reference 4. The solid symbols in figure 6 are calculated values based on theory given in reference 4 for zero cavitation number at a depth of submersion of 0.80 chord, the average depth of submersion for the present tests. Although in the present tests the hydrofoil was set at a constant depth of 6 inches ($d/c = 0.86$), the actual depths of submersion measured during the runs varied from $d/c = 0.58$ to $d/c = 1.02$ as a result of variations in the water level and of some unpredictable variations of strut rise under load. During a few runs made with the flat-bottomed hydrofoil mounted on the parabolic strut, the cavity pressure was measured and found not to be atmospheric (that is, $\sigma \neq 0$). These data points are also plotted in figure 6(a) (tailed solid symbols).

The dashed lines in figure 6 denote the approximate equation

$$C_{L,\sigma} = (1 + \sigma)C_{L,\sigma=0}$$

This equation is theoretically correct for very small values of σ. (See ref. 5.) Figure 6 shows that σ must be considerably less than 0.1 for the approximate equation to hold for angles of attack less than 20°. This marked deviation of the data from the approximate equation is in qualitative agreement with the complete two-dimensional solution given by Wu in reference 5.

The drag-coefficient values have been corrected to remove the drag of the strut by using aerodynamic-drag data for the strut section. However, photographic observation indicated that cavitation was occurring on the strut during most of the runs so that the strut drag would be expected to be greater than that predicted by aerodynamic data. Since the model used for these tests was the flat-bottomed hydrofoil, its drag should be given by $C_L \tan \alpha$ plus an increment due to friction (when

the top surface is not wetted). The dashed curves in the drag-coefficient plot in figure 6(a) are values thus obtained from faired experimental values of lift coefficient and a friction drag coefficient of 0.003. The difference between the two curves is believed to be caused by base drag resulting from cavitation on the strut.

A sudden drop in the lift and drag coefficients may be noted in the curve for an angle of attack of 20° at a cavitation number of about 0.26 (fig. 6). The discontinuity is also apparent in the moment plot, figure 7. This discontinuity is not believed to be caused by a reentrant flow at the rear of the cavity because, from figure 8, the cavity is expected to extend approximately 1 chord aft of the trailing edge of the model at this cavitation number. Also, pictures taken during these runs did not indicate that the top surface of the model was being wetted. As can be seen, no noticeable drop in lift or drag coefficient occurs at the other angles of attack. Since there is no apparent explanation for the discontinuity indicated by the data for the angle of attack of 20°, it is possible that this discontinuity does not exist but may be due to some experimental error.

The lift-coefficient data at an angle of attack of 4° for low cavitation numbers are considerably lower than the theoretical values for zero cavitation number because the top of the model was wetted over the forward half-chord at this angle of attack.

The theoretical values of center of pressure for $\sigma = 0$ shown in figure 7 are for angles of attack of 4° and 20° and indicate the spread over that range of angle of attack. The scatter of experimental data is rather large in comparison but tends to agree with theory as $\sigma = 0$ is approached except for the data at an angle of attack of 4°. At this angle of attack the upper surface of the model is wetted and thus is not completely within a cavity from the leading edge; therefore, the disagreement between theory and experiment is expected.

The variation of cavity length with cavitation number is shown in figure 8. The data were obtained by scaling from photographs taken by the above-water camera.

A comparison of cavitation numbers based on measured cavity pressure and on vapor pressure is shown in figure 9. As shown in reference 2, as the cavitation number increases the values of σ based on measured cavity pressure become increasingly smaller than those based on vapor pressure. This variation is due to the diffusion of dissolved gases into the cavity, with increased cavity pressure or decreased cavitation number as a result.

Typical photographs of the flat-bottomed hydrofoil operating at a finite cavitation number are shown in figure 10.

Zero Cavitation Number

The results of the tests made for the purpose of obtaining data at zero cavitation number are given in this section. As will be noted, in some cases, zero cavitation number was not realized, but even in such cases the cavitation number was usually small compared with those discussed in the previous section.

The lift, drag, pitching-moment, and center-of-pressure data obtained with the flat-bottomed and cambered hydrofoils operating at or near zero cavitation number are presented in figures 11 to 14 along with curves of theoretical values for lift, drag, and center of pressure. The theoretical values were calculated by the method given in reference 4. The theoretical drag coefficients include a friction drag coefficient of 0.003.

The trend of the data points in figures 11 and 13 seems to indicate that the lift coefficients are constant or increase slightly with an increase in depth of submersion. This trend is contradictory to that indicated by the theory, which shows a decrease in lift coefficient with an increase in depth. However, photographic observation indicated that the flow was not fully ventilated when the hydrofoils were operated at the deeper depths. Photographs illustrating fully and partially ventilated flows about the hydrofoils are presented in figure 15. The wake aft of the strut is seen to be much shorter for the partially vented condition (figs. 15(b) and (d)) than for the fully vented condition (figs. 15(a) and (c)). An approximate border between the fully and the partially vented flow conditions determined by photographic observations is indicated on the lift-coefficient plots in figures 11 and 13. Thus, the data points in the partially vented region actually represent cavitation numbers slightly greater than zero. Therefore, the lift coefficients in this region would be expected to be greater than those predicted by theory.

A limited number of runs were made with the flat-bottomed hydrofoil with a brass tube fastened to the rear of the parabolic strut (fig. 2) in an unsuccessful attempt to improve the ventilation characteristics of the configuration. It was hoped that complete ventilation could be established by breaking up the thin wisp of spray originating at the junction of the strut with the free-water surface. This spray was believed to be sealing off the cavity aft of the strut and thus preventing airflow to the hydrofoil cavity. The tube also was used for measuring the pressure in the cavity during these runs and the results obtained are included in figure 11 with the measured cavitation number noted beside each data point on the lift-coefficient plot. The same data have also been plotted in figure 6(a) as previously noted (tailed solid symbols), where the order of increase from the zero-cavitation-number value may be noted.

The center-of-pressure data (figs. 12 and 14) show fairly good agreement with theory.

Lift-drag ratios.- The variation of lift-drag ratio with depth of submersion for both hydrofoils is shown in figure 16. As shown, the lift-drag ratios vary little with depth of submersion at high angles of attack. The lift-drag ratio increases with a decrease in angle of attack, as expected, until the flow starts to attach to the upper surface of the model. At this point, for the flat-bottomed hydrofoil, a sudden drop in lift-drag ratio occurs because of the loss in lift. A more gradual drop occurs for the cambered model because of the curvature of the upper surface of the model. Theory indicates that the decrease in lift-drag ratio will become more pronounced with increase in depth of submersion as a result of the leading-edge spray jet becoming attached to the upper surface of the model at higher angles of attack.

A direct comparison of lift-drag ratios for the two hydrofoils at a constant depth of submersion is shown in figure 17. The data symbols (fig. 17(a)) indicate crossplotted values of lift coefficient and lift-drag ratio for $d/c = 0.40$. The advantage of the cambered hydrofoil over the flat-bottomed hydrofoil is shown in figure 17(a) where the lift-drag ratio is plotted against lift coefficient. As seen, the values of the lift-drag ratio are nearly the same for the two hydrofoils at given angles of attack above the minimum angle of attack (angle at which the top surface is wetted for each hydrofoil) but occur for the cambered lifting surface at considerably larger lift coefficients. A plot of lift-drag ratio against angle of attack is presented in figure 17(b) and shows directly the similarity in lift-drag ratios for given angles of attack. As indicated by the values of lift-drag ratio, the minimum angle of attack occurs between 4° and 5° for the flat-bottomed hydrofoil and at about 7° for the cambered hydrofoil. A much more abrupt drop in lift-drag ratio would be expected for the flat-bottomed hydrofoil than for the cambered hydrofoil, since the upper surface of the flat-bottomed hydrofoil is made up of flat sections, the total forward half-chord would be wetted at once which would result in an appreciable loss in lift and increase in drag, whereas the extent to which the upper surface of the cambered hydrofoil would be wetted would increase gradually with a decrease in angle of attack.

The cambered hydrofoil has a smaller maximum lift-drag ratio than the flat-bottomed hydrofoil because of the large amount of camber used (two-dimensional design lift coefficient of 0.392) which restricts the ventilated range of the hydrofoil to relatively high angles of attack. That a better maximum lift-drag ratio can be obtained with a cambered section than with the flat-bottomed hydrofoil is shown in figure 23 of reference 7. One of the hydrofoils discussed in the reference has a circular-arc section which closely approximates the Tulin-Burkart section of the present hydrofoil. As indicated in the reference, the

maximum lift-drag ratio increases with design lift coefficient until (with the wedge angle at the leading edge kept constant) a design lift coefficient slightly greater than 0.1 is reached. Further increase in camber for that section resulted in a decrease in maximum obtainable lift-drag ratio.

Spray thickness.- The variation of spray thickness with depth of submersion is shown in figure 18 for both hydrofoils. As the depth increases, the value of δ/c approaches that of d/c, and for depths greater than 0.4 chord, the two values are about equal.

Cavity spray height.- The variation of the height of the undersurface of the leading-edge spray jet above the reference line with depth of submersion is shown in figures 19 and 20. The data presented in figure 19 were obtained with the probe mechanism. The path of the probe (always vertical) with respect to the hydrofoil chord varied with angle of attack. (See sketch in fig. 19.) The readings of spray heights presented in figure 19 represent distances from the position where the probe path would intersect the hydrofoil reference line. The values of spray height presented in figure 20 represent distances from the hydrofoil reference line measured along the trailing edge of the strut (perpendicular to the reference line) and were obtained from photographs taken with the overhead camera.

A comparison of experimental and theoretical values of spray height for the two hydrofoils is presented in figure 21. The theoretical values were calculated by the method given in reference 7. Since no theoretical expression was available for the relation between d/c and δ/c, the calculations of spray height were first based on the assumption that $\delta/c = d/c$. The spray-height values were later recalculated based on δ/c by using the experimentally determined relationship between d/c and δ/c (fig. 18) and both sets of curves are shown in figure 21. As may be noted, there is an appreciable difference in the results of the two sets of calculations at high angles of attack and low values of d/c, but the difference becomes fairly small at angles of 8° or less even at shallow depths. Although theory and experiment do not agree at high angles of attack, the agreement improves with decreasing angle so that theory gives a good indication of the minimum angle of attack for which the top surface of the hydrofoil is not wetted. A comparison of both the theoretical and experimental values of spray height for the two models indicates that camber changes the spray contour very little, especially at the lower angles of attack.

The values of spray height obtained from photographs may be seen to be slightly lower than those obtained from the probe mechanism. This is caused by the change in spanwise curvature of the spray due to the effect of the strut supporting the hydrofoil. That is, instead of the spanwise curvature of the cavity having a roughly elliptical shape with

the maximum height at the midspan, the cavity height is reduced at the center because of the effect of the strut resulting in a somewhat heart-shaped spanwise curvature. This effect is illustrated in a photograph taken during a run that was made with the flat-bottomed hydrofoil with three pins attached to its upper surface. A sketch of the configuration and the photograph taken during the run are shown in figure 22. The inboard and outboard pins may be seen to extend into the spray while the middle pin does not. The indication of spray position given by the middle pin agrees with the probe data as may be seen in the plot for $\alpha = 16^{\circ}$ in figure 21. (The path of the probe was located approximately 1/4 inch inboard of the middle pin.)

Flow details.- A series of photographs is presented in figure 23 to show the variation of flow about the hydrofoils with angle of attack. The top surface of the flat-bottomed hydrofoil is wetted at an angle of attack of 4° but a tendency for the flow to separate from the leading edge may be noted as the depth is decreased from $d/c = 0.58$ to $d/c = 0.14$ (fig. 23(a)). This tendency is in fair agreement with theory (fig. 21(a)), which predicts that the flow would be separated at $d/c = 0.25$ for an angle of attack of 4°. The roughness of the spray from the leading edge is due to leading-edge vibration.

A photograph of flow about the cambered hydrofoil for $\alpha = 9^{\circ}$ (fig. 23(b)) indicates that the flow is attached to the top surface but tending to separate. (The depths of submersion were not obtained for angles of attack of 9° and 10° in fig. 23(b) because of record failure, but the hydrofoil was set for a constant depth of $d/c = 0.5$ at the start of each run.) The flow is still attached to the upper surface for a short distance aft of the leading edge of the hydrofoil at $\alpha = 10^{\circ}$. The results indicated by these photographs agree fairly well with theory (fig. 21(b)), which indicates separation of flow at $\alpha = 10^{\circ}$ for values of d/c less than 0.25 and at $\alpha = 12^{\circ}$ for $d/c = 0.5$ or less.

A zero-cavitation-number flow is generally considered to be a flow in which only positive pressure coefficients exist. If this concept is true, any wetting of the upper surface must decrease the lift-drag ratio. However, the photographs indicated that the top surface of the cambered hydrofoil was partially wetted at angles of attack less than 10° whereas the lift-drag ratio (fig. 17) kept increasing with decrease in angle of attack to 7°. Evidently, at finite speeds, some wetting of the top surface is tolerable and may even be beneficial when the top surface of the model has proper chordwise curvature. This may be better explained with the aid of the sketches of different regimes of flow shown in figure 24. Figure 24(a) illustrates the flow condition commonly associated with zero cavitation number (that is, the pressure in the cavity is approximately vapor pressure and the hydrofoil velocity is infinite). In the present tests, the zero-cavitation-number

condition was simulated at finite speeds by causing the flow to be ventilated. As stated in references 7 and 8, in any flow about a body where a region of separation exists, the fluid in the separated region may be replaced by any lighter fluid by providing a means for the lighter fluid to flow into the separated region. This was done in the present tests, as illustrated in figure 24(b), by using a blunt-trailing-edge strut to provide a passage for air to flow into the separated region and thus to vent the top surface of the hydrofoil to the atmosphere. Then, for angles of attack where the separation region begins at the leading edge, the vented cavity on the hydrofoil will also originate from the leading edge and the flow will be similar to that shown in figure 24(a). The cavitation number based on cavity pressure for the condition shown in figure 24(b) is also zero because the cavity pressure p_c is, for practical purposes, equal to the local pressure p_o. Since the flows are similar and the cavitation numbers are identical, the laws for calculating forces and moments are the same for figures 24(a) and (b).

Another flow regime is encountered at finite speeds as the angle of attack is decreased and the stagnation point moves to the leading edge. Leading-edge separation no longer occurs although separation may occur at some location downstream of the leading edge depending on the shape of the upper surface. This type of separation may result from either of two causes: boundary-layer separation or vapor cavitation. When air is introduced to this separated region, a vented flow such as that shown in figure 24(c) results. Typical pressure distributions on the upper surface of the hydrofoil, with flow separation caused by cavitation, are shown in the inset of figure 24(c) for the two representative speeds. The dashed lines represent the pressure distribution for an ideal fluid not subject to cavitation. In the real case this ideal distribution is modified as shown by the solid lines in the inset; when the local pressure reaches vapor pressure, a vapor cavity forms which immediately is vented to the atmosphere downstream. This phenomenon results in the discontinuous pressure distribution shown. It may be noted that as speed is increased, the negative pressure region decreases in length whereas the positive pressure region remains approximately constant. Thus, at infinite speed, any wetting of the upper surface would be detrimental to the hydrodynamic efficiency.

Leading-edge vibration.- A photograph of the flow indicating leading-edge vibration is shown in figure 25 for the flat-bottomed hydrofoil. The flat-bottomed hydrofoil used in these tests showed a tendency for leading-edge vibration at angles of attack of 12° or less. No evidence of leading-edge vibration was noted for the cambered hydrofoil over the ranges of angles of attack and speed tested.

CONCLUSIONS

Conclusions based on the results of the experimental investigation of a flat-bottomed and a cambered supercavitating hydrofoil may be summarized as follows:

1. The theory for predicting forces and moments for supercavitating hydrofoils of arbitrary camber, aspect ratio, and depth of submersion at zero cavitation number produces results in good agreement with experiment.

2. The simple equation $C_{L,\sigma} = (1 + \sigma)C_{L,\sigma=0}$ for predicting the lift coefficient is not adequate except for very small cavitation numbers.

3. As the depth of submersion of the leading edge of the hydrofoil increases, the value of spray thickness approaches the value for depth of submersion and for depths greater than 0.4 chord the two values are about equal.

4. Theory and experiment are not in agreement for spray contours at high angles of attack but the agreement improves with decreasing angle and theory gives a good indication of the minimum angle of attack for which the top surface of the hydrofoil is not wetted.

5. At finite speeds, the lift-drag ratio of a supercavitating hydrofoil does not necessarily decrease as soon as the upper surface becomes wetted. In fact, if the upper surface has proper chordwise curvature, an appreciable area may be wetted before the lift-drag ratio starts to decrease.

Langley Research Center,
National Aeronautics and Space Administration,
Langley Field, Va., September 9, 1959.

REFERENCES

1. King, Douglas A., and Land, Norman S.: Effects of Sweepback and Taper on the Force and Cavitation Characteristics of Aspect-Ratio-4 Hydrofoils. NACA RM L52J10, 1952.

2. Kermeen, Robert W.: Water Tunnel Tests of NACA 4412 and Walchner Profile 7 Hydrofoils in Noncavitating and Cavitating Flows. Rep. No. 47-5 (Contract Nonr-220(12)), Hydrod. Lab., C.I.T., Feb. 1956.

3. Tulin, M. P., and Burkart, M. P.: Linearized Theory for Flows About Lifting Foils at Zero Cavitation Number. Rep. C-638, David W. Taylor Model Basin, Navy Dept., Feb. 1955.

4. Johnson, Virgil E., Jr.: Theoretical and Experimental Investigation of Arbitrary Aspect Ratio, Supercavitating Hydrofoils Operating Near the Free Water Surface. NACA RM L57I16, 1957.

5. Wu, T. Yao-tsu: A Free Streamline Theory for Two-Dimensional Fully Cavitated Hydrofoils. Rep. No. 21-17 (Contract N6onr-24420), Hydrod. Lab., C.I.T., July 1955.

6. Christopher, Kenneth W.: Investigation of the Planing Lift of a Flat Plate at Speeds up to 170 Feet Per Second. NACA TN 3951, 1957.

7. Johnson, Virgil E., Jr.: The Influence of Depth of Submersion, Aspect Ratio, and Thickness on Supercavitating Hydrofoils Operating at Zero Cavitation Number. Presented at Second Symposium on Naval Hydrod. (Washington), Aug. 1958.

8. Wadlin, Kenneth L.: Mechanics of Ventilation Inception. Presented at the Second Symposium on Naval Hydrod. (Washington), Aug. 1958.

TABLE I

DATA FOR FLAT-BOTTOMED HYDROFOIL MOUNTED ON STREAMLINED STRUT

[Density of tank water, 1.941 slugs/cu ft]

(a) Data from Langley high-speed hydrodynamics facility

V, fps	d/c	C_L	C_D	$C_{m,c/4}$	C_{cp}	σ_c	σ_v
			$\alpha = 20^\circ$				
148.65	0.83	0.322	0.133	-0.034	0.347	0.096	0.099
108.14	.98	.367	.145	-.050	.375	.179	.186
99.39	1.02	.392	.155	-.059	.390	.213	.220
91.86	.87	.412	.162	-.061	.388	.250	.257
118.50	.76	.351	.138	-.049	.380	-----	-----
110.16	.81	.352	.139	-.050	.382	.186	.179
101.74	.81	.382	.147	-.061	.399	.220	.212
166.99	.75	.303	.121	-.037	.362	.076	.079
154.18	.76	.313	.125	-.043	.378	.090	.092
142.63	.73	.321	.128	-.040	.365	.105	.108
88.13	.94	.386	.152	-.043	.355	.264	.281
80.64	.94	.414	.161	-.052	.356	.308	.336
			$\alpha = 16^\circ$				
112.77	0.74	0.308	0.093	-0.038	0.367	0.166	0.172
102.73	.68	.334	.108	-.041	.367	.201	.207
94.64	.74	.360	.113	-.049	.379	.237	.244
100.50	.89	.337	.108	-.044	.375	-----	-----
92.81	.82	.363	.114	-.051	.385	.239	.252
85.85	.75	.397	.121	-.064	.403	.276	.294
155.79	.94	.255	.085	-.025	.341	.087	.089
144.25	.80	.268	.091	-.025	.340	.102	.104
134.35	.77	.275	.093	-.025	.338	.117	.120
162.04	1.02	.243	.077	-.010	.287	.082	.083
149.61	1.01	.251	.078	-.012	.297	.096	.097
			$\alpha = 12^\circ$				
164.03	0.79	0.192	0.047	-0.020	0.350	0.081	0.080
151.87	.78	.203	.057	-.012	.306	.094	.094
141.55	.93	.211	.056	-------	-----	.108	.108
103.34	.80	.285	.073	-.033	.363	.187	.204
96.63	.81	.311	.079	-.041	.377	.215	.234
90.72	.75	.339	.085	-.048	-----	.242	-----
			$\alpha = 8^\circ$				
93.13	0.77	0.299	0.055	-0.049	0.412	0.242	0.251
86.70	.79	.336	.060	-.057	.418	-----	-----
81.98	.77	.347	.060	-.060	.419	.309	.324
101.79	.58	.248	.049	-.033	.342	.192	.212
94.14	.64	.292	.055	-.046	.404	.226	.248
87.72	.62	.330	.059	-.057	.341	.256	.286
136.12	.58	.165	.034	-.016	.348	.116	.119
125.30	.67	.182	.037	-.020	.357	-----	-----
116.87	.63	.200	.038	-.027	.381	.158	.161
168.17	.57	.135	.032	-.009	.316	.077	.078
155.50	.60	.145	.035	-.009	.308	-----	-----
145.58	.59	.152	.036	-.0003	.252	.103	.104
			$\alpha = 4^\circ$				
151.10	0.67	0.039	0.021	-0.007	0.420	-----	-----
140.49	.68	.038	.024	-.010	.512	0.112	0.112
129.23	.66	.039	.026	-.019	.721	.129	.132
84.07	.63	.202	.034	-.065	.568	.271	.312
77.75	.66	.214	.034	-.061	.533	.316	.366
71.89	.65	.211	.030	-.056	.512	.369	.428

TABLE I.- Concluded

DATA FOR FLAT-BOTTOMED HYDROFOIL MOUNTED ON STREAMLINED STRUT

(b) Data from Langley tank No. 2

α, deg	V, fps	d/c	C_L	C_D	σ_c	σ_v
19.71	59.17	0.85	0.667	0.248	0.533	0.624
19.68	63.56	.85	.595	.224	.471	.541
19.61	73.68	.85	.481	.185	.364	.403
15.74	64.33	.85	.576	.167	.406	.528
15.73	69.85	.85	.503	.149	.350	.448
15.71	73.96	.85	.460	.138	.322	.400
11.74	69.44	.85	.492	.106	.422	.453
11.72	74.19	.85	.459	.101	.352	.397
11.71	78.70	.85	.412	.095	.315	.353

TABLE II

DATA FOR FLAT-BOTTOMED HYDROFOIL MOUNTED ON PARABOLIC STRUT

[Density of tank water, 1.941 slugs/cu ft]

V, fps	d/c	C_L	C_D	$C_{m,c/4}$	C_{cp}	σ_c
			$\alpha = 30^\circ$			
135.57	0.33	0.409	0.244	-------	-----	
126.40	.35	.411	.245	-------	-----	
117.91	.34	.411	.243	-------	-----	
			$\alpha = 20^\circ$			
141.74	0.34	0.262	0.105	-0.014	0.299	
129.11	.32	.270	.107	-.015	.300	
117.82	.16	.267	.111	-.004	.262	
160.07	.55	.279	.103	-------	-----	
148.87	.27	.286	.107	-------	-----	
139.77	.05	.299	.111	-------	-----	
138.10	.51	.262	.103	-.014	.301	
			$\alpha = 16^\circ$			
168.86	0.55	0.217	0.066	-0.014	0.310	
155.80	.51	.220	.065	-.012	.301	
144.35	.31 .31	.222	.067	-.016	.318	
165.12	.74	.222	.073	-.011	.296	
151.15	.62	.208	.067	-.0004	.252	
138.05	.51	.208	.067	-.001	.253	
169.81	.21	.213	.069	-.011	.301	
154.90	.12	.222	.072	-.011	.297	
141.05	.02	.233	.075	-.010	.292	
			$\alpha = 14^\circ$			
163.19	0.72	0.194	0.058	-0.009	0.293	
148.11	.60	.202	.063	-.006	.280	
135.19	.55	.207	.064	-.007	.282	
			$\alpha = 12^\circ$			
164.75	0.49	0.161	0.041	-0.005	0.279	
150.74	.35	.160	.041	-.004	.274	
139.31	.21	.154	.042	-.001	.247	
168.15	.62	.157	.035	-.010	.309	
156.34	.63	.156	.031	-.013	.329	
146.07	.48	.157	.031	-.015	.346	
153.00	.68	.195	.046	-------	-----	
138.83	.53	.186	.043	-------	-----	
133.36	.36	.168	.039	-------	-----	
173.74	.27	.155	.040	-.005	.283	
159.62	.16	.160	.041	-.004	.274	
147.05	.03	.166	.042	-.005	.279	
176.97	.77	.166	.044	-.003	.265	
160.02	.67	.173	.046	-.002	.263	
144.63	.54	.165	.044	-.001	.254	
			$\alpha = 10^\circ$			
162.29	0.40	0.132	0.028	-0.004	0.278	
149.10	.21	.133	.030	-.003	.268	
138.30	.03	.135	.031	-.003	.269	

TABLE II.- Concluded

DATA FOR FLAT-BOTTOMED HYDROFOIL MOUNTED ON PARABOLIC STRUT

V, fps	d/c	C_L	C_D	$C_{m,c/4}$	C_{cp}	σ_c
			$\alpha = 8^\circ$			
157.27	0.42	0.122	0.023	-0.004	0.286	
144.22	.28	.108	.021	-.0002	.252	
133.57	.10	.104	.021	-.001	.262	
171.75	.35	.115	.022	-.005	.294	
157.09	.32	.122	.023	-.005	.290	
146.52	.21	.102	.018	0	.250	
168.93	.37	.108	.019	-.003	.279	
157.43	.25	.105	.018	-.002	.264	
147.24	.17	.105	.018	-.003	.280	
164.5	.79	.126	.021	-------	-----	
152.04	.64	.123	.022	-------	-----	
139.63	.51	.126	.023	-------	-----	
181.95	.82	.113	.021	-.014	.301	
163.00	.73	.117	.023	.001	.242	
146.94	.64	.119	.022	-.004	.285	
181.24	.27	.120	.024	-.013	.355	
163.75	.21	.105	.021	-.016	.395	
147.98	.21	.109	.020	-.014	.373	
163.65	.83	.112	.021	.002	.234	0.035
149.33	.71	.116	.023	.003	.223	.039
135.48	.58	.112	.022	.022	.232	.038
			$\alpha = 7^\circ$			
159.14	0.35	0.104	0.018	-0.001	0.259	
147.71	.31	.095	.015	-.001	.255	
137.29	.22	.092	.015	.0001	.249	
			$\alpha = 6^\circ$			
147.51	0.30	0.089	0.013	0.0004	0.246	
136.77	.21	.080	.012	.002	.223	
			$\alpha = 5^\circ$			
162.87	0.38	0.074	0.010	-0.005	0.310	
150.27	.29	.084	.010	-.004	.299	
138.51	.21	.087	.011	-.005	.301	
			$\alpha = 4^\circ$			
166.63	0.36	0.043	0.009	-0.013	0.549	
155.21	.30	.048	.008	-.002	.281	
145.18	.24	.053	.008	-.001	.265	
163.50	.79	.033	.009	-------	-----	
151.30	.70	.036	.010	-------	-----	
139.22	.58	.035	.010	-------	-----	
168.19	.90	.018	.009	.035	.218	0.030
153.49	.79	.022	.011	.033	.140	.031
140.26	.69	.024	.016	.028	.210	.027
185.38	.29	.043	.009	-.0001	.252	.017
166.78	.22	.051	.011	.003	.200	.028
152.19	.14	.057	.010	-.003	.302	.024
			$\alpha = 3^\circ$			
170.26	0.36	0.014	0.006	-0.005	0.578	
159.28	.32	.021	.007	-.004	.439	
149.19	.32	.026	.007	-.003	.346	

TABLE III

DATA FOR CAMBERED HYDROFOIL MOUNTED ON PARABOLIC STRUT

[Density of tank water, 1.941 slugs/cu ft]

V, fps	d/c	C_L	C_D	$C_{m,c/4}$	C_{cp}
		$\alpha = 20^\circ$			
143.99	0.38	0.431	0.168	------	-----
132.92	.27	.433	.171	------	-----
122.46	.30	.434	.169	------	-----
168.70	.78	.434	.158	------	-----
155.34	.50	.429	.155	------	-----
142.09	.39	.434	.156	------	-----
147.52	.50	.411	.153	-0.083	0.439
135.77	.18	.406	.150	-.087	.450
150.67	.28	.408	.153	-.073	.417
136.42	.02	.419	.158	-.072	.411
161.70	.52	.400	-----	------	-----
148.76	.13	.416	-----	------	-----
		$\alpha = 16^\circ$			
158.12	0.35	0.378	0.123	------	-----
146.02	.23	.383	.125	------	-----
134.42	.23	.386	.126	------	-----
170.50	.37	.381	.110	------	-----
157.02	.33	.385	.114	------	-----
144.20	.40	.388	.114	------	-----
146.94	.57	.376	.117	-0.075	0.440
132.30	.17	.343	.105	-.069	.441
156.60	.33	.362	.110	-.071	.438
142.67	.11	.376	.113	-.080	.455
		$\alpha = 12^\circ$			
161.34	0.37	0.324	0.081	------	-----
148.00	.33	.328	.083	------	-----
136.89	.28	.328	.080	------	-----
162.69	.95	.341	.086	------	-----
151.25	.86	.349	.089	------	-----
172.60	.77	.353	.084	------	-----
160.66	.68	.362	.088	------	-----
149.01	.49	.364	.089	------	-----
152.28	.31	.304	.072	-0.064	0.455
136.41	.27	.314	.076	-.065	.452
123.03	.24	.315	.076	-.067	.456
164.79	.84	.328	.079	-.068	.452
148.45	.67	.342	.085	-.069	.446
134.39	.53	.349	.086	-.072	.450
172.31	.49	.309	.073	-.065	.455
155.11	.46	.311	.075	-.065	.452
140.57	.48	.306	.075	-.060	.442
		$\alpha = 10^\circ$			
166.58	0.46	0.300	0.065	------	-----
152.59	.41	.302	.065	------	-----
140.73	.29 .28	.303	.064	------	-----
159.38	.84	.320	.073	------	-----
147.84	.78	.328	.075	------	-----
137.14	.73	.332	.077	------	-----
166.99	.63	.303	.066	------	-----
154.18	.35	.313	.063	------	-----
142.63	.22	.321	.063	------	-----
169.96	[a].5	.284	-----	------	-----
154.80	[a].5	.287	-----	------	-----
139.55	[a].5	.288	-----	------	-----
170.64	.43	.285	.058	-0.068	0.483
155.57	.44	.291	.060	-.062	.458
141.01	.43	.295	.061	-.063	.458

[a] d/c value estimated.

TABLE III.- Concluded

DATA FOR CAMBERED HYDROFOIL MOUNTED ON PARABOLIC STRUT

V, fps	d/c	C_L	C_D	$C_{m,c/4}$	C_{cp}
		$\alpha = 9^\circ$			
172.51	[a]0.5	0.285	-----	------	-----
158.60	[a].5	.289	-----	------	-----
145.74	[a].5	.304	-----	------	-----
178.95	.43	.279	0.054	-0.060	0.460
159.24	.44	.284	.055	-.059	.453
143.35	.44	.285	.056	-.060	.456
172.49	.40	.281	.053	-.061	.466
159.85	.41	.284	.054	-.062	.464
149.11	.26	.287	.057	-.062	.459
		$\alpha = 8^\circ$			
172.05	0.47	0.284	0.052	------	-----
158.16	.41	.297	.053	------	-----
146.03	.30	.303	.063	------	-----
144.87	.52	.288	.054	-0.069	0.485
128.94	.46	.291	.056	-.069	.483
115.72	.44	.302	.057	-.074	.489
173.34	.51	.276	.049	-.067	.489
156.92	.46	.286	.054	-.066	.478
142.52	.42	.290	.056	-.069	.483
171.56	..52	.274	.052	-.072	.508
153.64	.53	.287	.056	-.070	.489
137.65	.52	.292	.056	-.071	.488
180.49	.44	.271	.048	-.063	.480
162.39	.47	.280	.049	-.062	.470
146.99	.47	.283	.049	-.063	.491
		$\alpha = 7^\circ$			
169.23	0.39	0.259	0.040	-0.067	0.505
153.13	.33	.263	.043	-.062	.482
137.97	.31	.267	.043	-.064	.486
143.71	.48	.258	.047	-.071	.522
133.57	.51	.264	.048	-.071	.516
124.96	.52	.269	.050	-.073	.516
176.03	.47	.246	.044	-.066	.514
156.93	.47	.255	.045	-.065	.500
141.02	.49	.258	.044	-.068	.512
		$\alpha = 6^\circ$			
180.43	0.39	0.226	0.037	-0.068	0.546
162.96	.31	.234	.038	-.065	.526
147.63	.24	.239	.040	-.067	.527
171.34	.52	.213	.043	-.030	.389
154.52	.48	.224	.043	-.043	.439
140.44	.48	.233	.041	-.065	.526

[a] d/c value estimated.

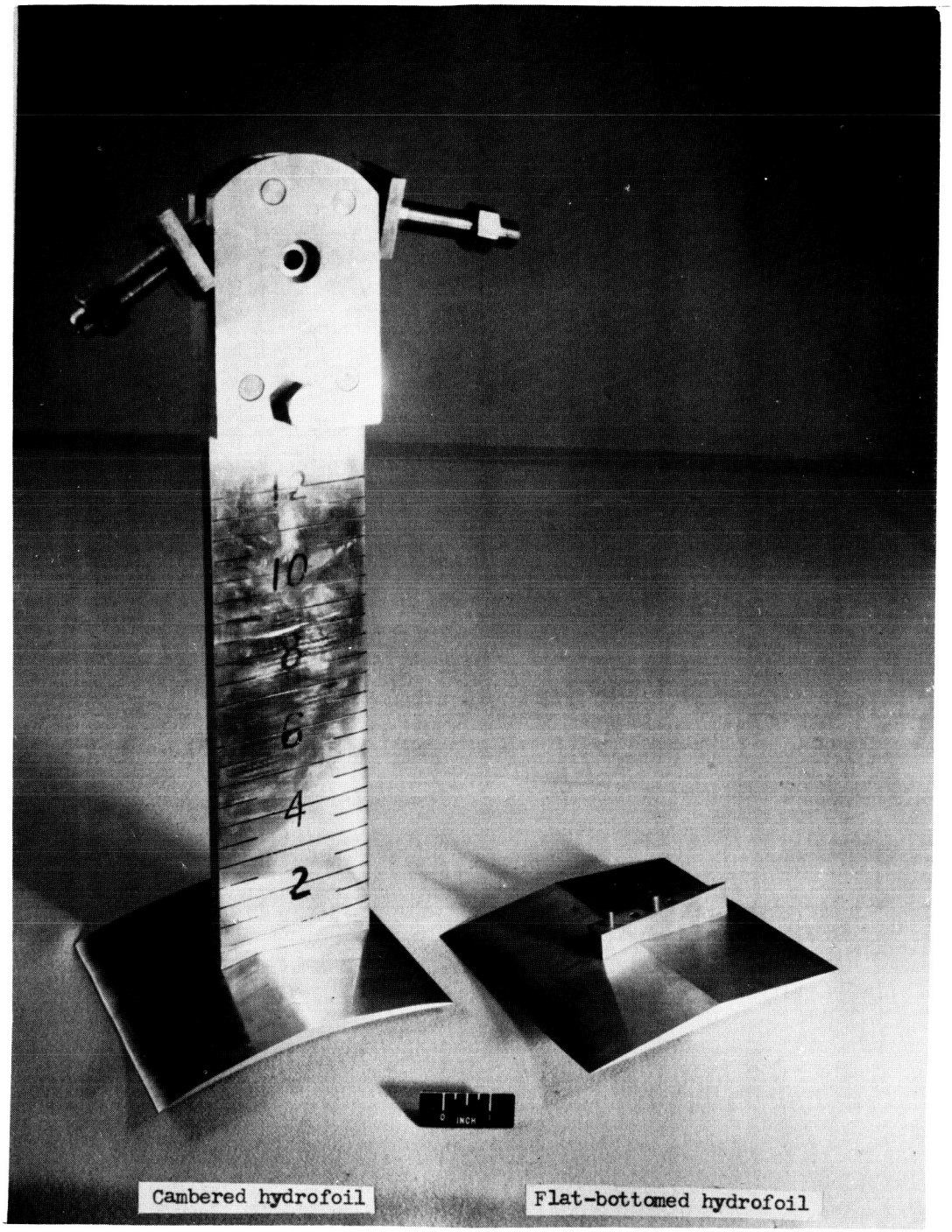

L-58-1460.1

Figure 1.- Photograph of hydrofoils and parabolic strut.

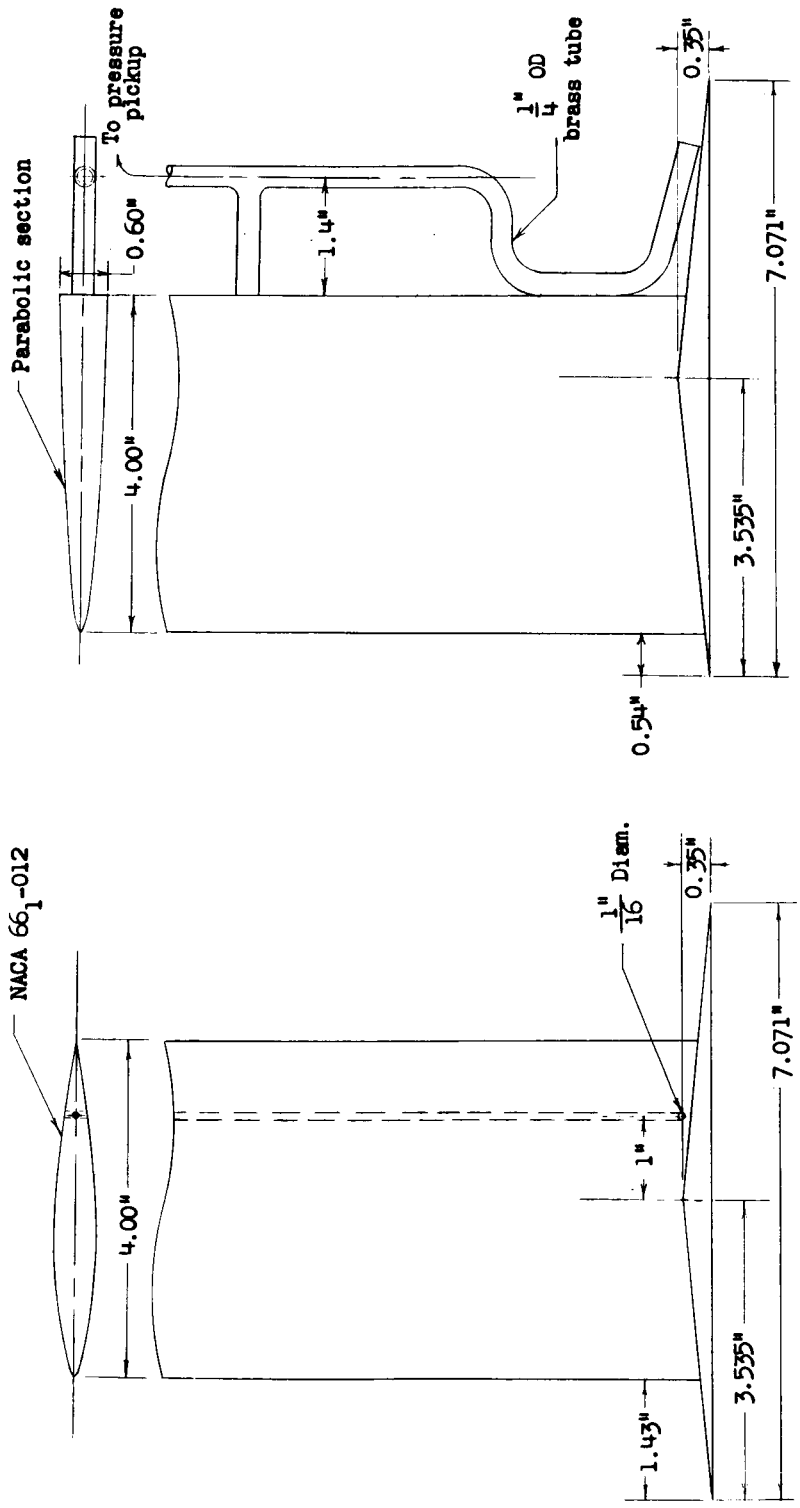

Figure 2.- Drawing of flat-bottomed hydrofoil attached to streamlined and parabolic struts with systems for measuring cavity pressure.

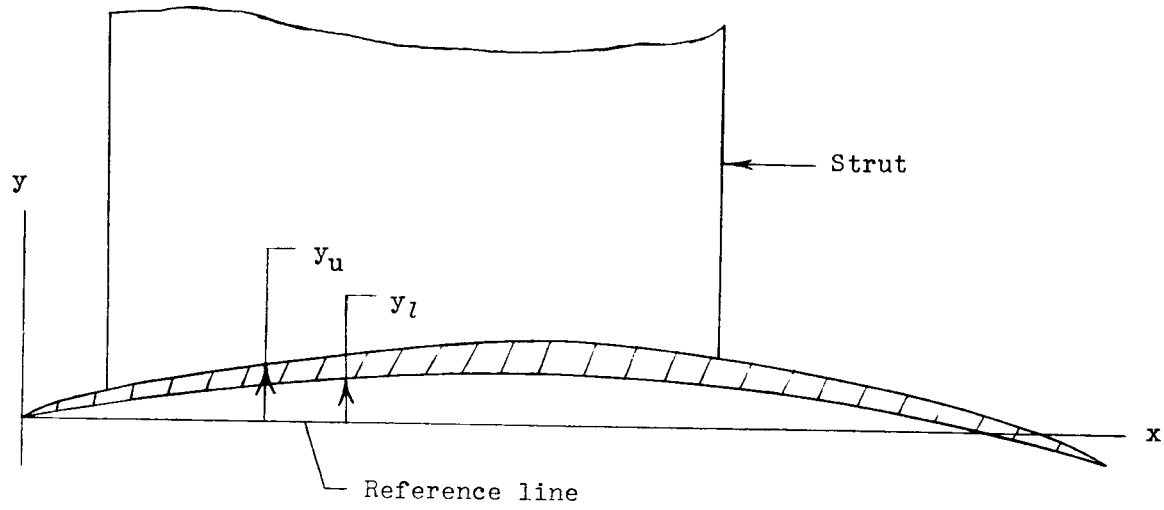

x, in.	y_u, in.	y_l, in.	x, in.	y_u, in.	y_l, in.
0	0	0	3.75	0.536	0.308
0.25	.092	.037	4.00	.502	.297
0.50	.155	.071	4.25	.467	.282
0.75	.207	.108	4.50	.430	.262
1.00	.253	.144	4.75	.390	.237
1.25	.292	.177	5.00	.349	.207
1.50	.327	.207	5.25	.302	.172
1.75	.363	.234	5.50	.254	.132
2.00	.396	.257	5.75	.206	.088
2.25	.426	.277	6.00	.150	.038
2.50	.456	.293	6.25	.084	-.018
2.75	.483	.305	6.50	.010	-.078
3.00	.511	.312	6.75	-.079	-.144
3.25	.536	.315	7.00	-.189	-.215
3.50	.550	.314	7.071	-.236	-.236

Figure 3.- Profile and coordinates for cambered hydrofoil.

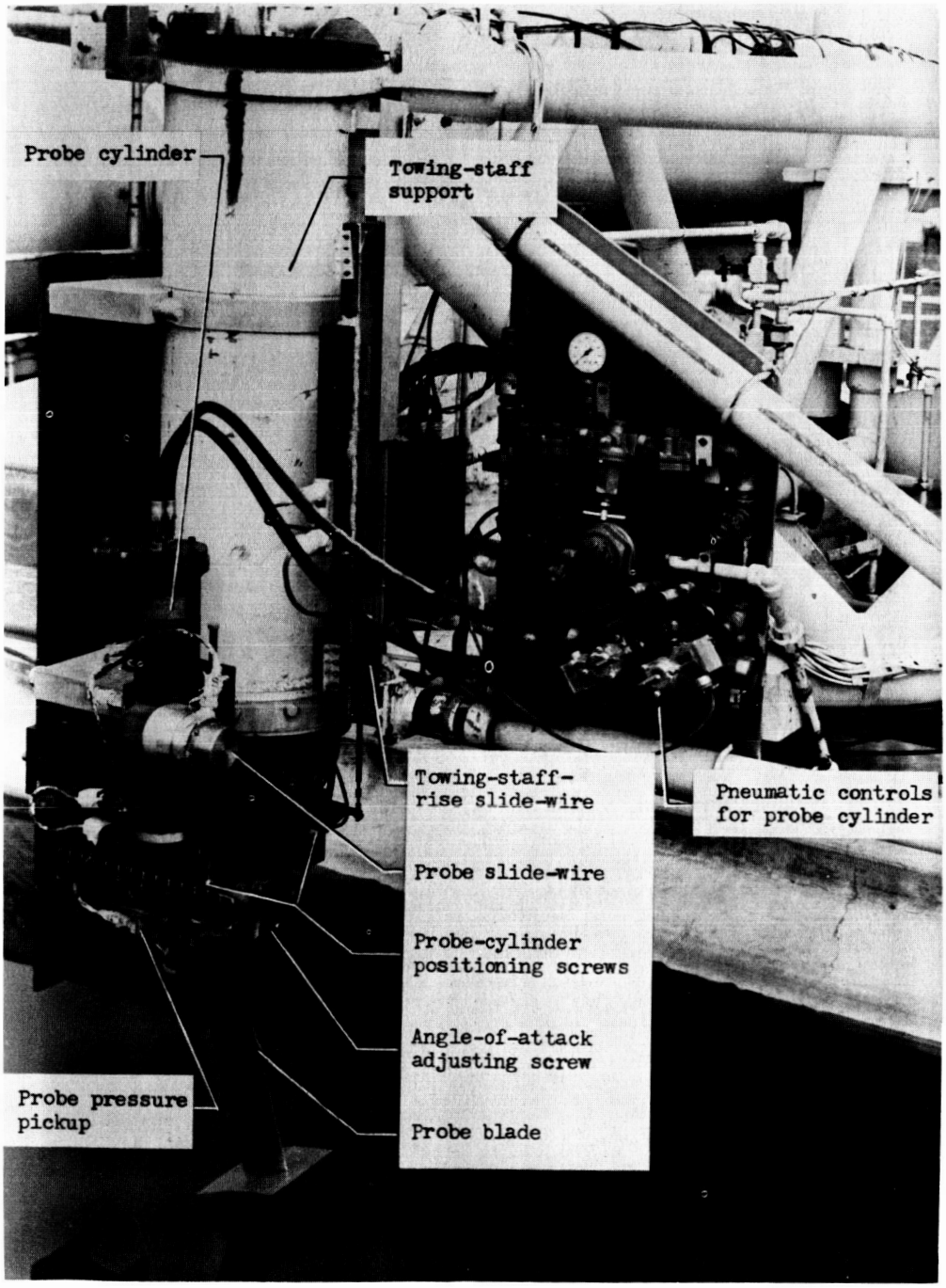

L-58-3531.1

Figure 4.- Test setup showing flat-bottomed hydrofoil mounted on streamlined strut.

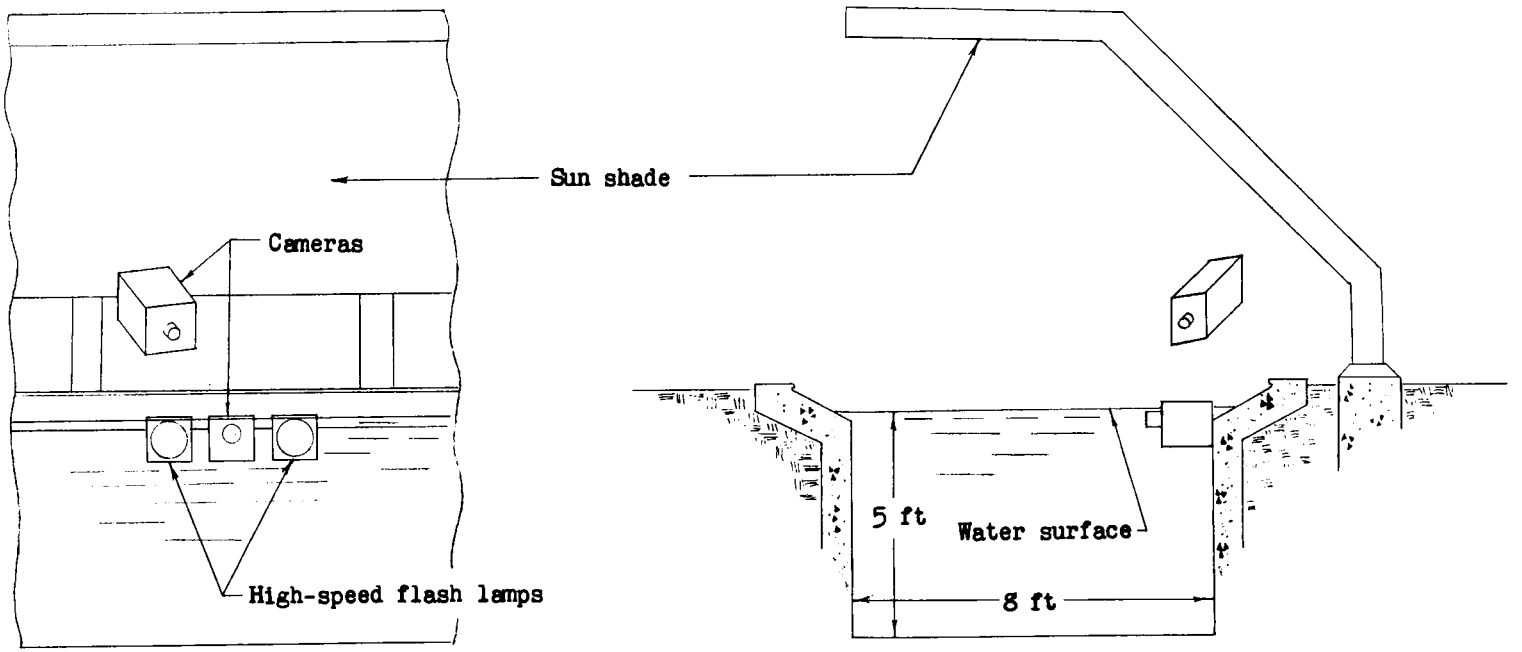

(a) Longitudinal section.

(b) Transverse section.

Figure 5.- Sections of tank at a photographic station.

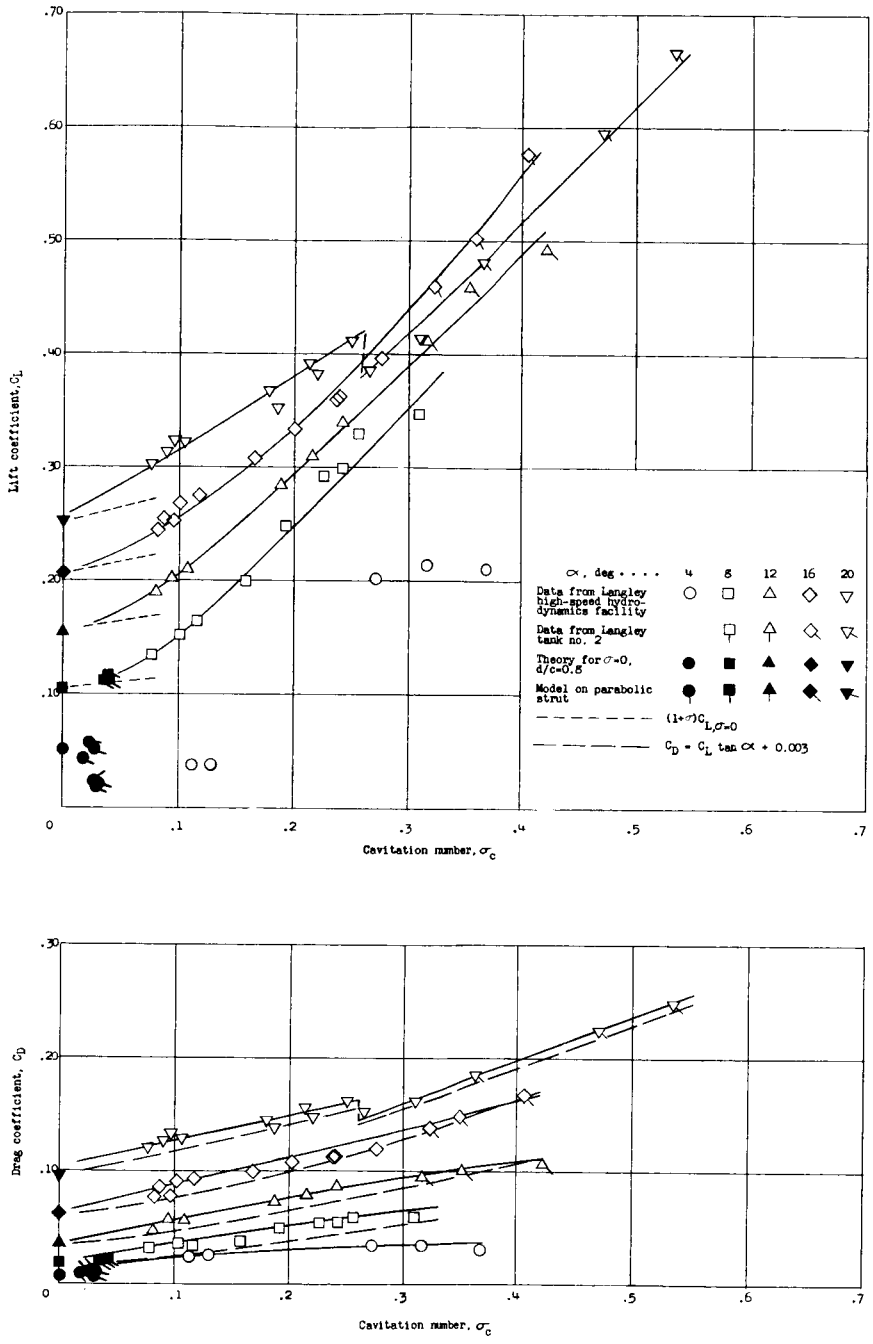

(a) Cavitation number based on cavity pressure.

Figure 6.- Variation of lift and drag coefficient with cavitation number for flat-bottomed hydrofoil.

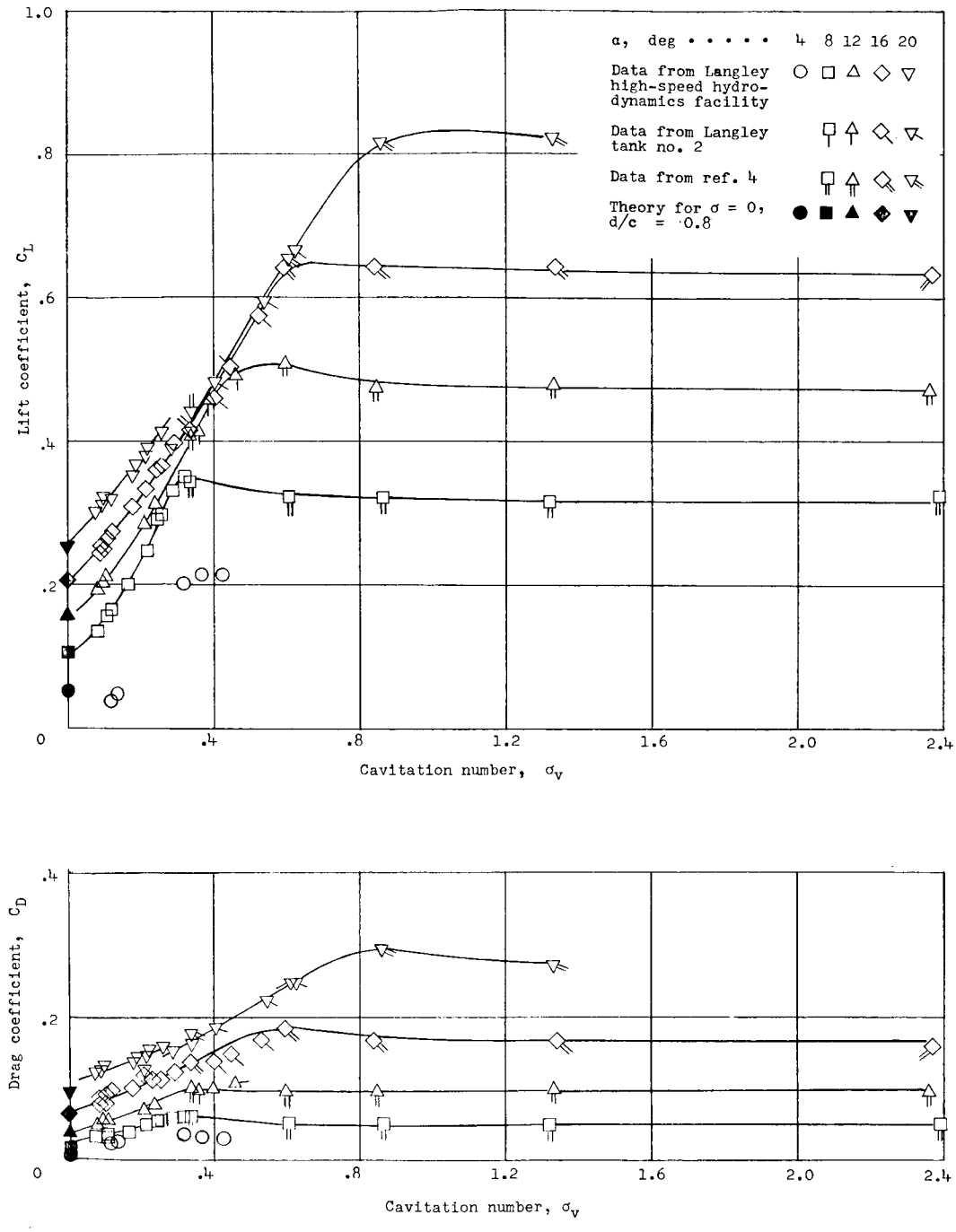

(b) Cavitation number based on vapor pressure.

Figure 6.- Concluded.

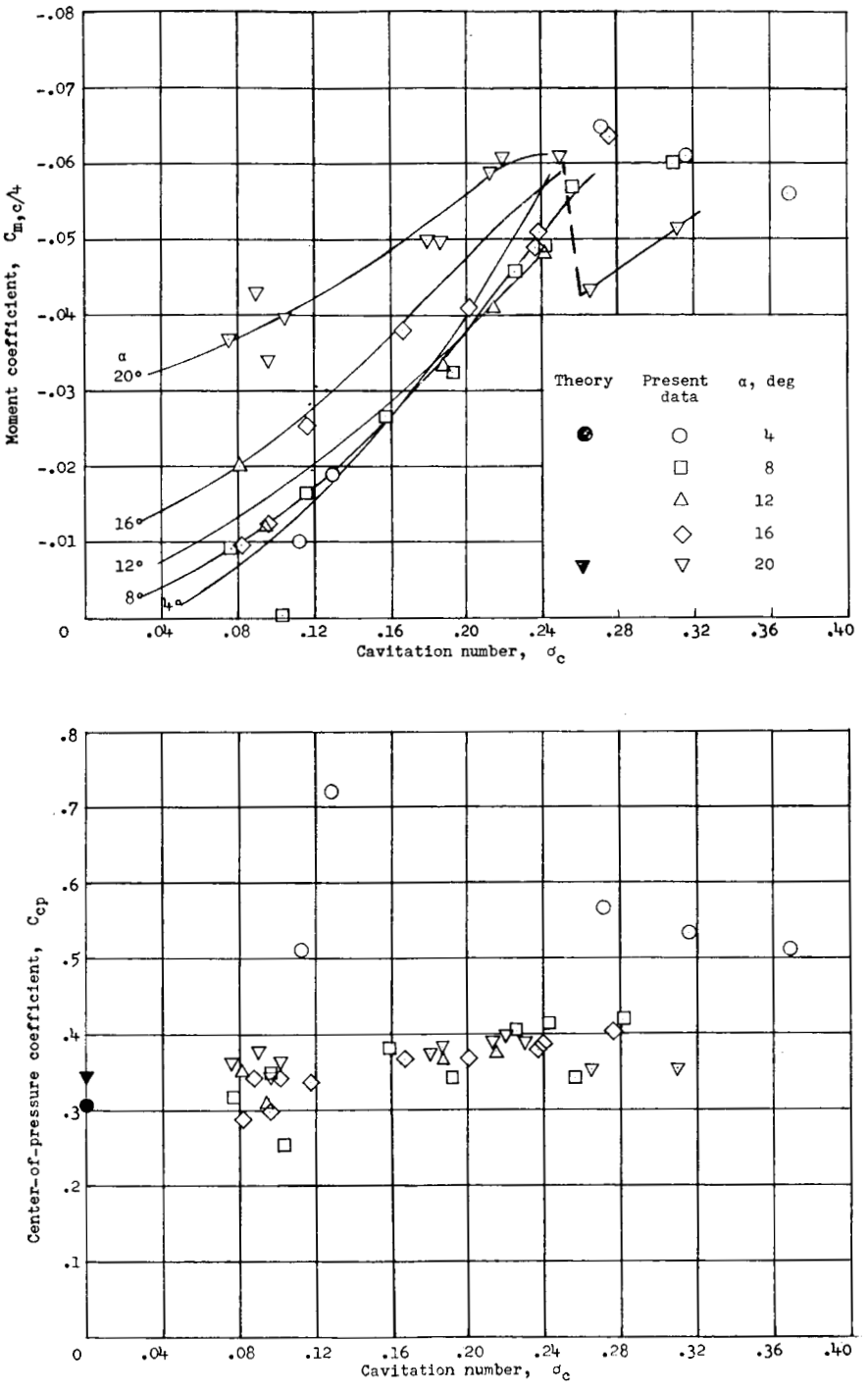

Figure 7.- Variation of moment coefficient and center-of-pressure coefficient with cavitation number for flat-bottomed hydrofoil.

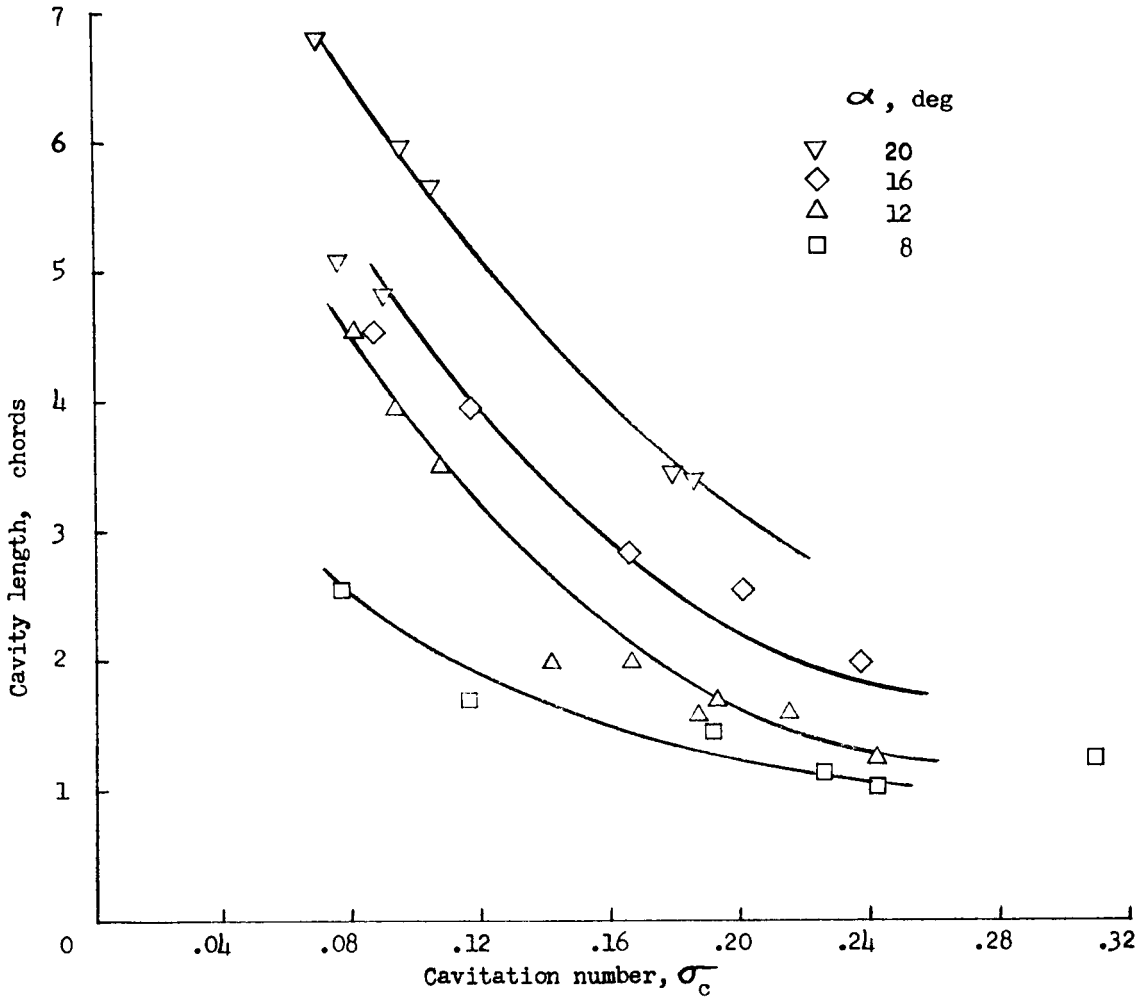

Figure 8.- Variation of length of cavity with cavitation number based on cavity pressure for flat-bottomed hydrofoil.

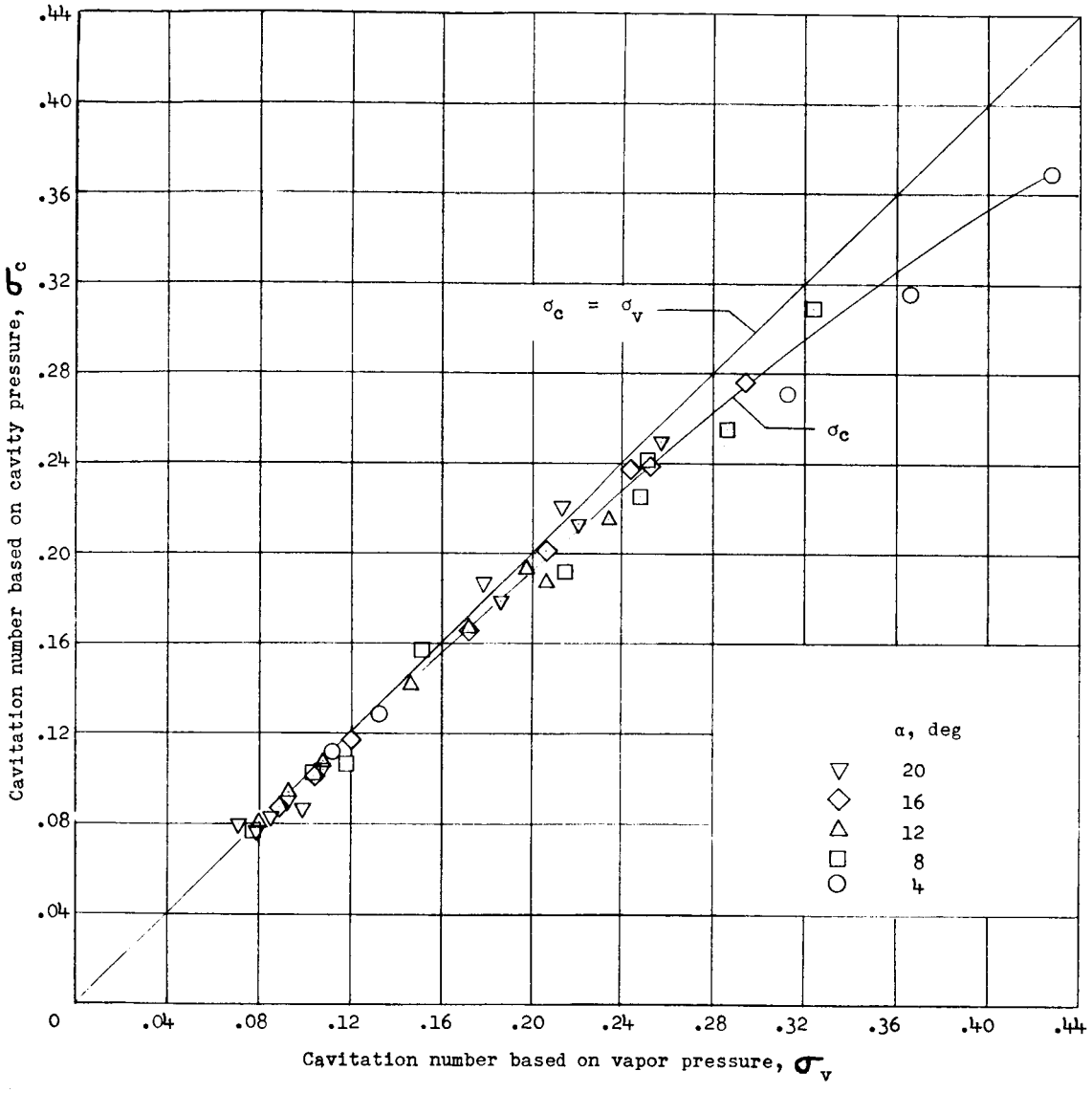

Figure 9.- Comparison of cavitation number based on measured cavity pressure with cavitation number based on vapor pressure for flat-bottomed hydrofoil.

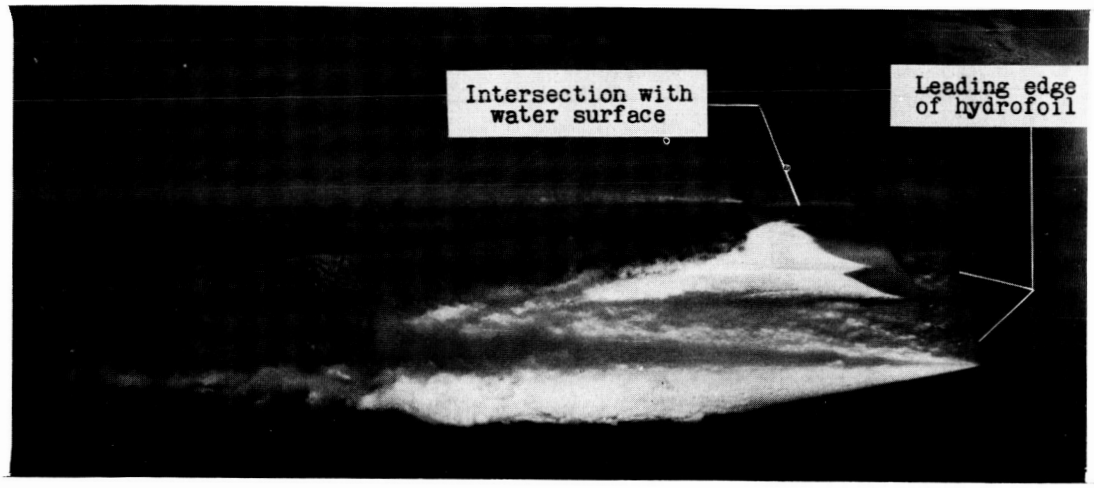

(a) Overhead camera.

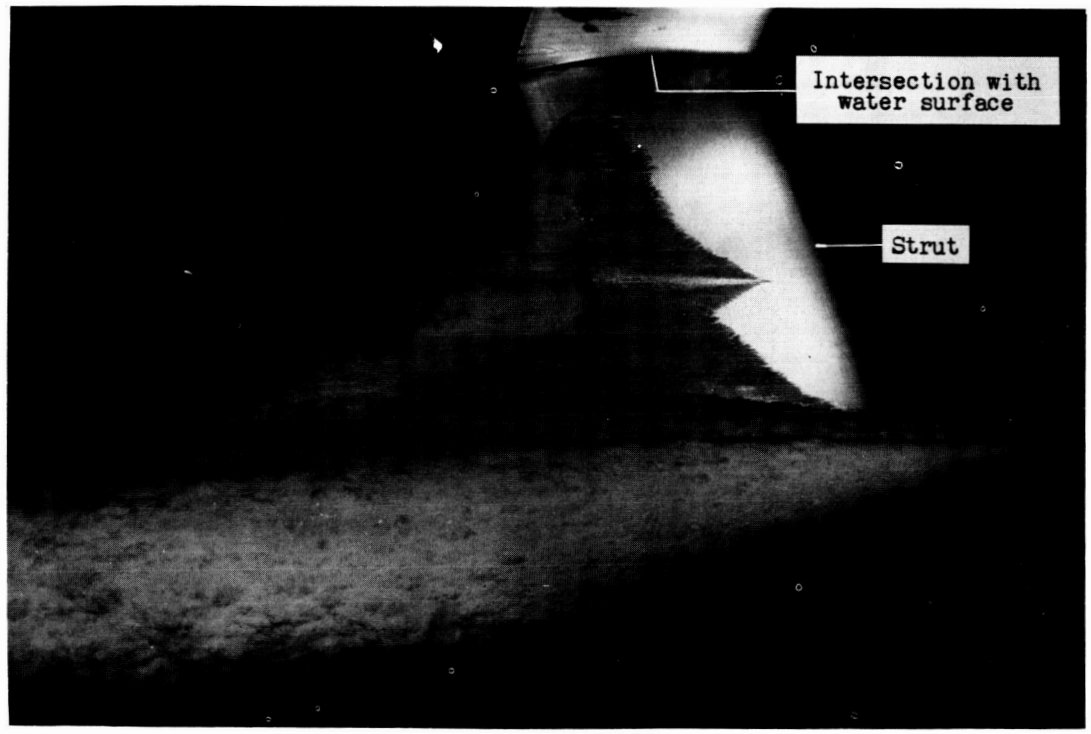

(b) Underwater camera. L-59-6072

Figure 10.- Flow about flat-bottomed hydrofoil at finite cavitation number. $\alpha = 20^{\circ}$; $d/c = 0.81$; $\sigma_c = 0.186$.

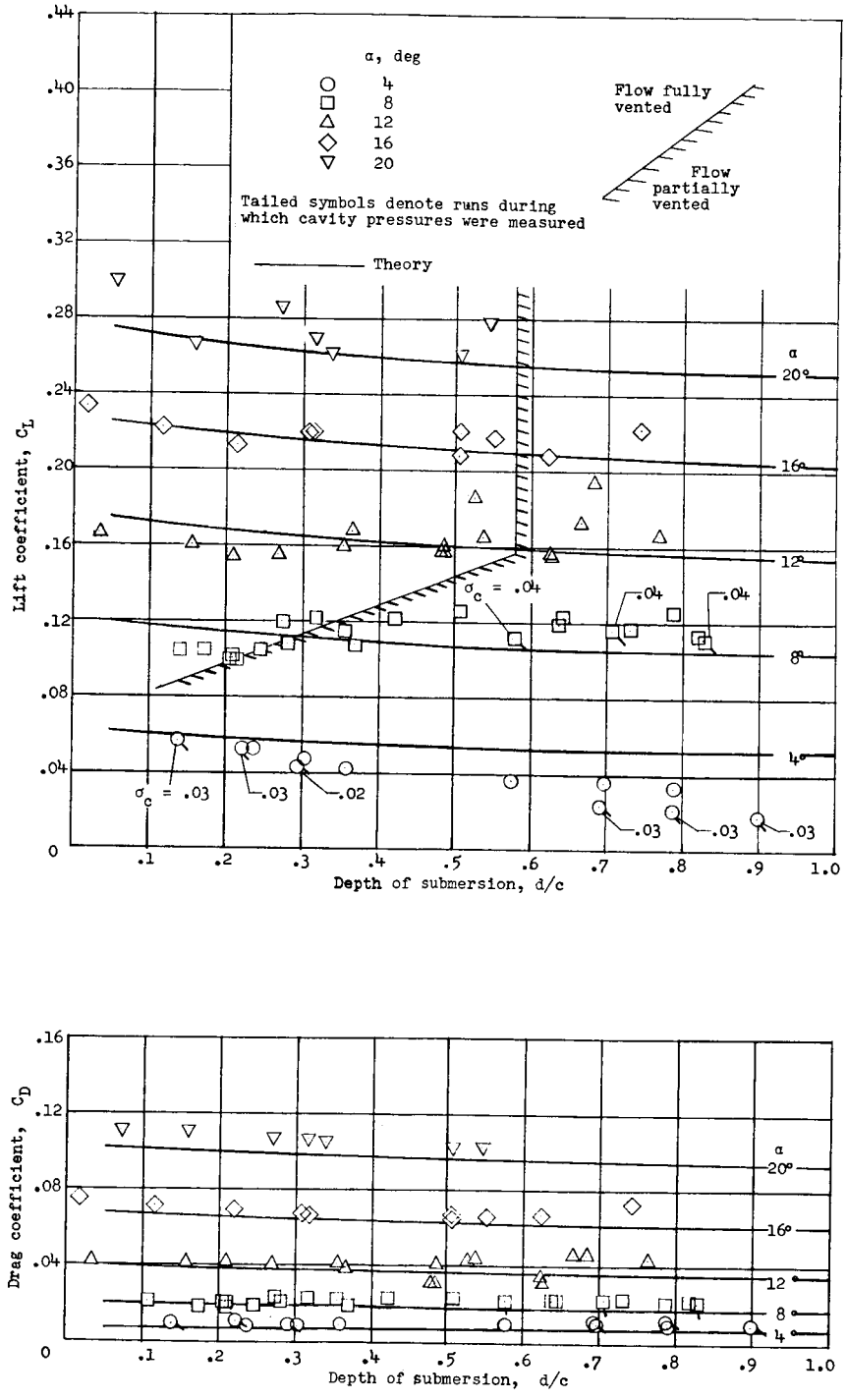

Figure 11.- Variation of lift and drag coefficients with depth of submersion for flat-bottomed hydrofoil at or near zero cavitation number.

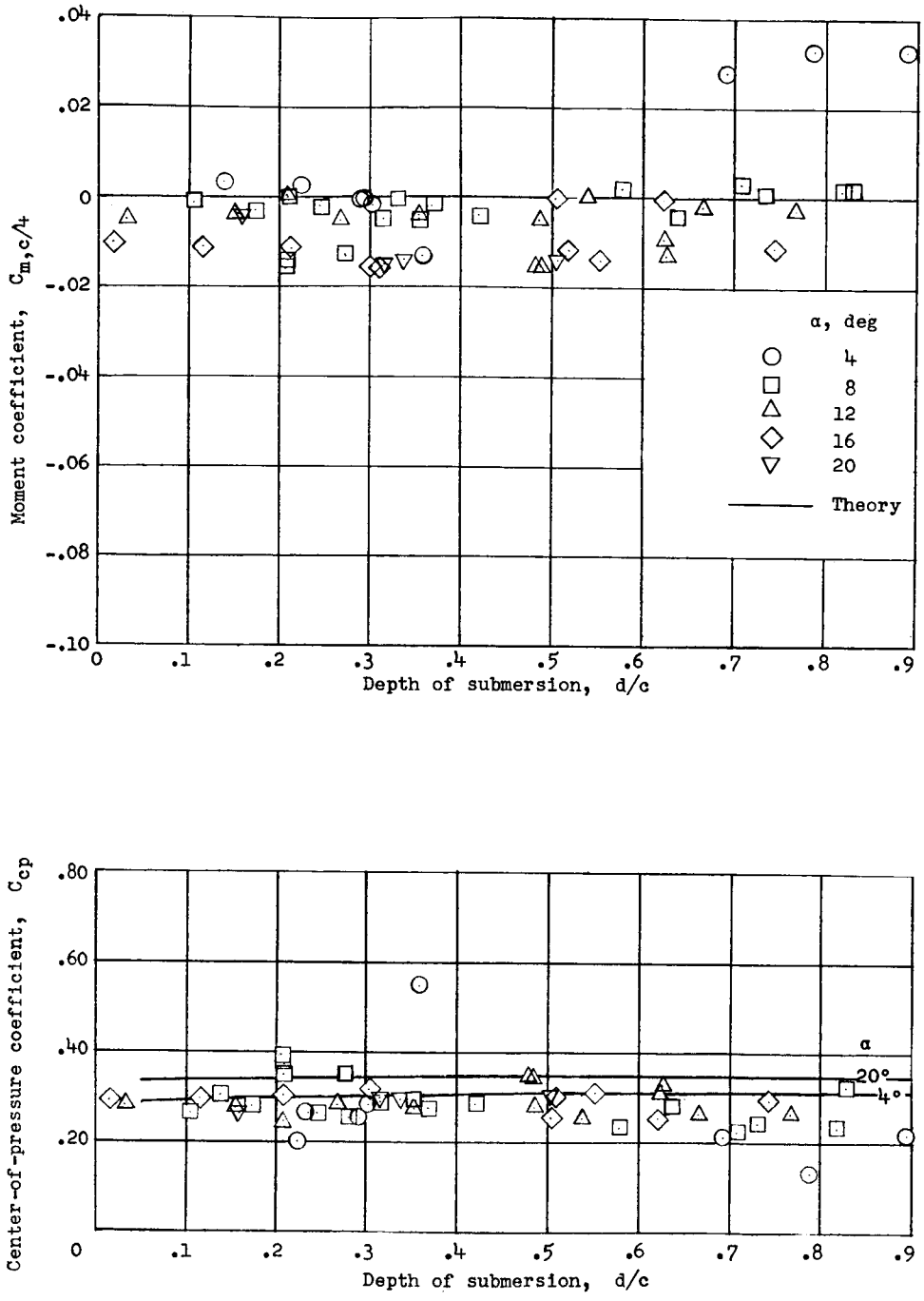

Figure 12.- Variation of moment coefficient and center-of-pressure location with depth of submersion for flat-bottomed hydrofoil at or near zero cavitation number.

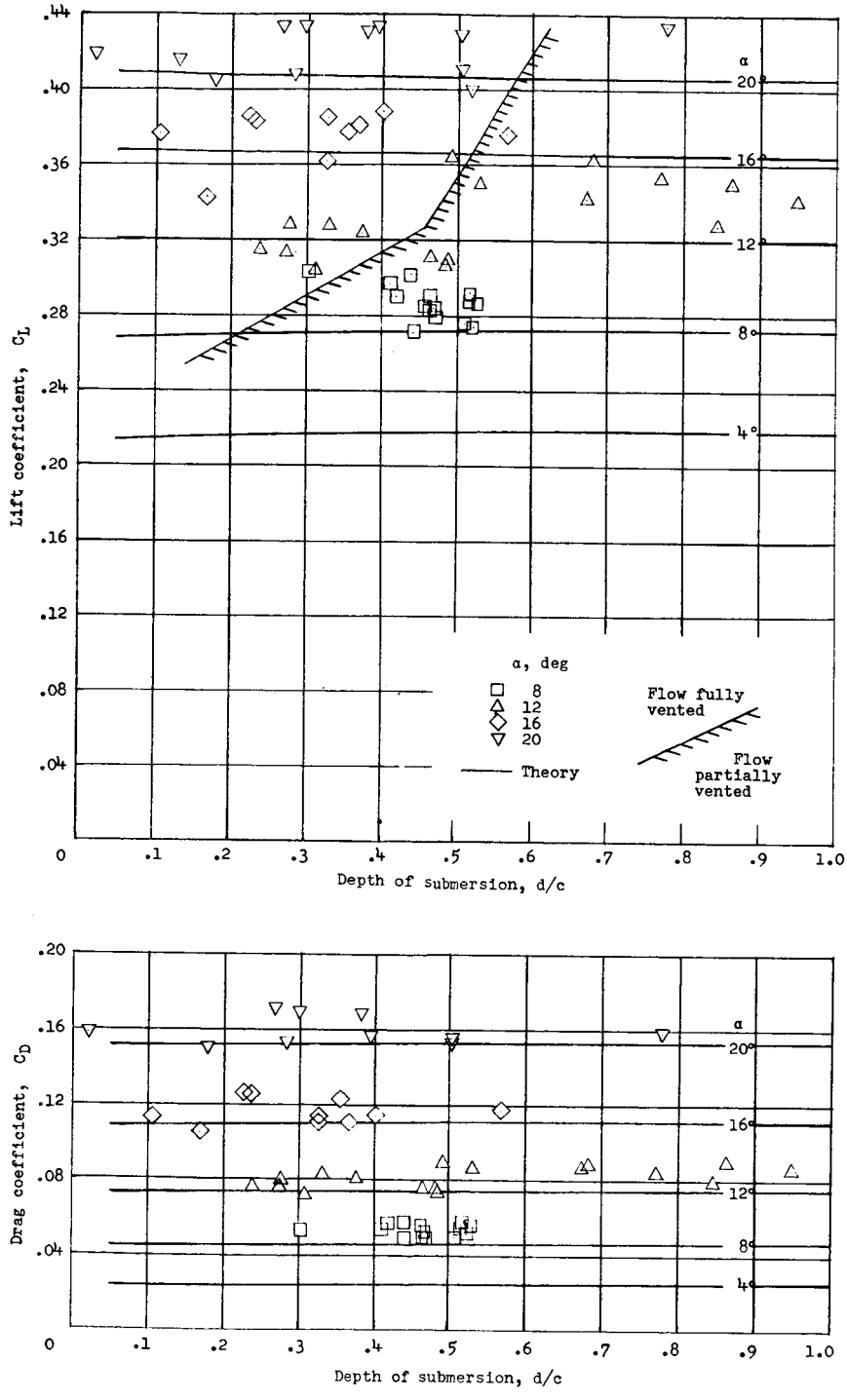

Figure 13.- Variation of lift and drag coefficients with depth of submersion for cambered hydrofoil at or near zero cavitation number.

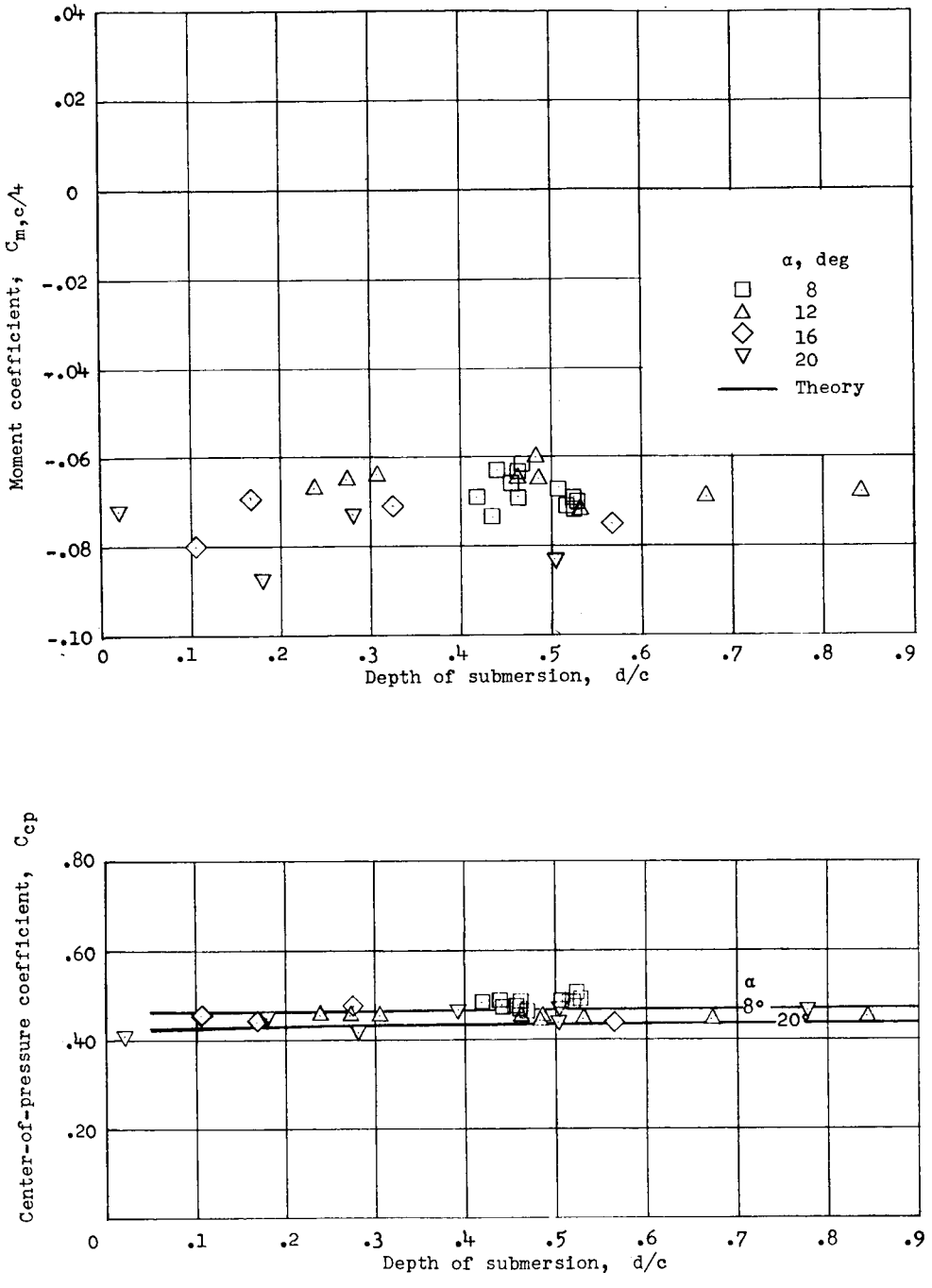

Figure 14.- Variation of moment coefficient and center-of-pressure location with depth of submersion for cambered hydrofoil at or near zero cavitation number.

Overhead camera

Underwater camera

L-59-6073

(a) Flat-bottomed hydrofoil; fully vented. $\alpha = 20^{\circ}$; $d/c = 0.51$; $V = 138.10$ fps.

Figure 15.- Photographs of flow about lifting surfaces indicating fully and partially vented conditions.

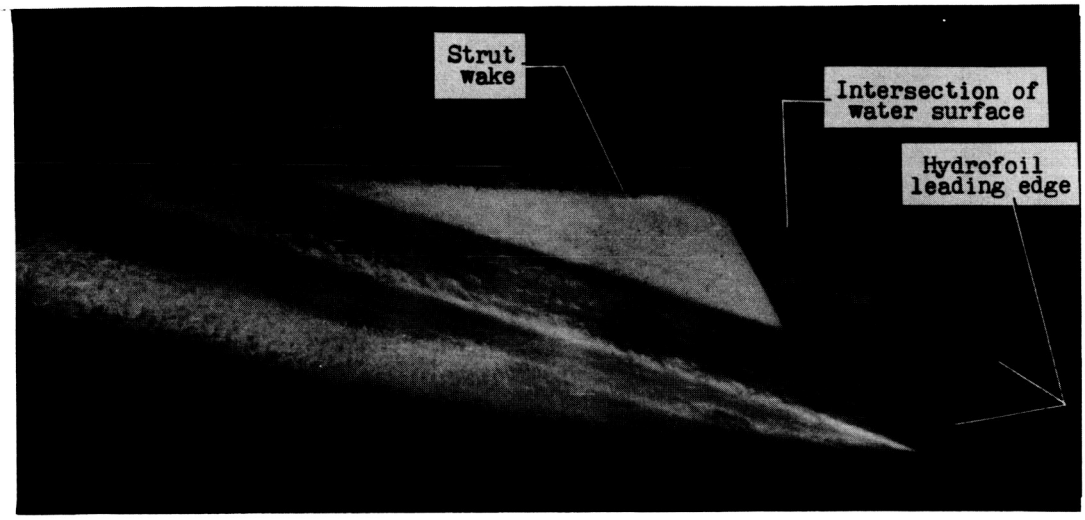

Overhead camera

Underwater camera

L-59-6074

(b) Flat-bottomed hydrofoil; partially vented. $\alpha = 20^{\circ}$; $d/c = 0.68$; $V = 153.21$ fps.

Figure 15.- Continued.

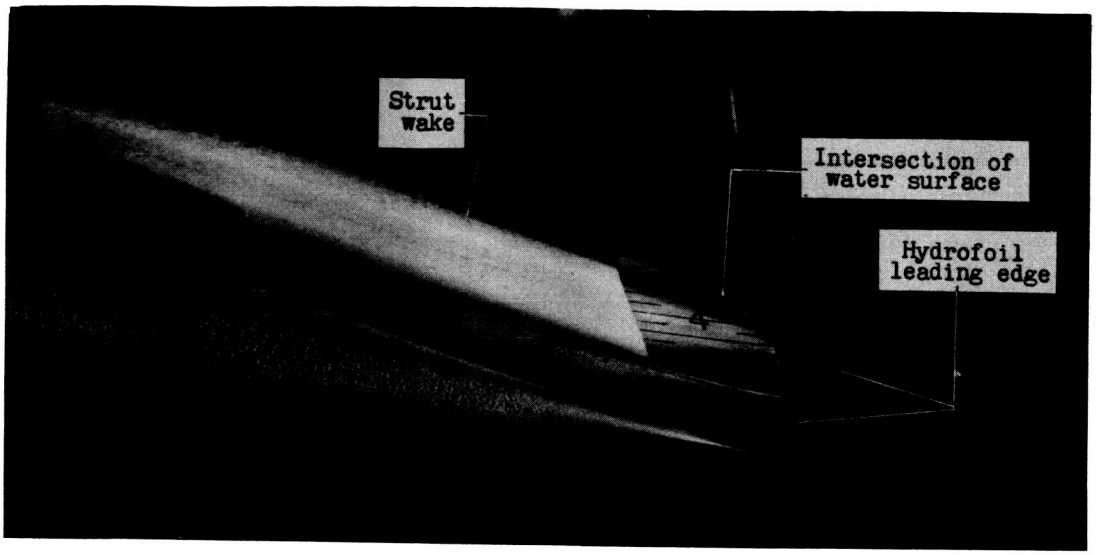

Overhead camera

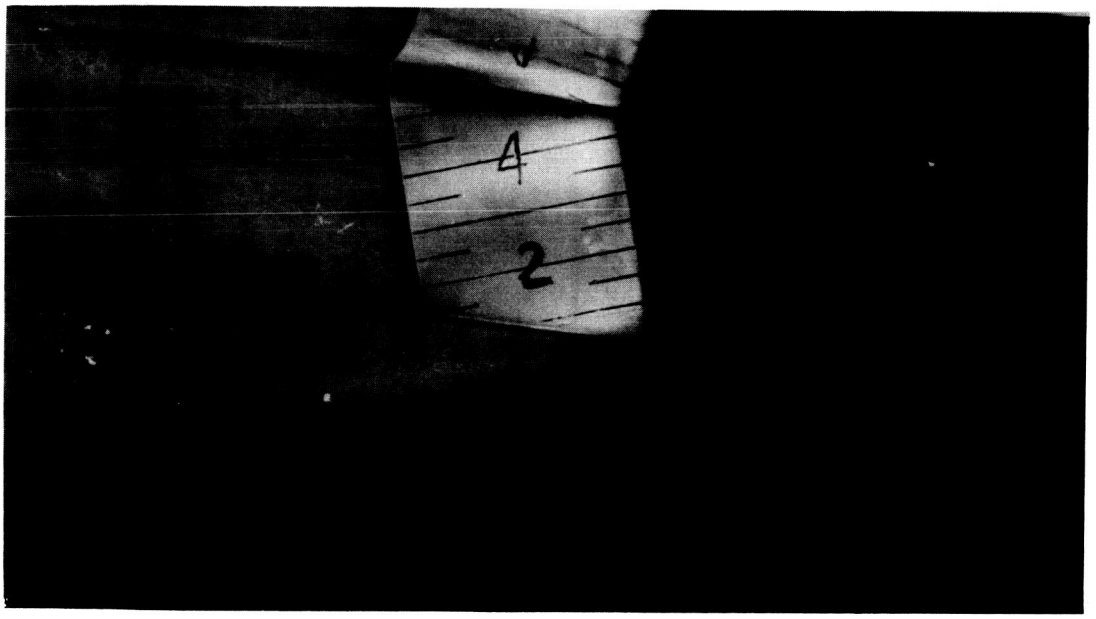

Underwater camera

L-59-6075

(c) Cambered hydrofoil; fully vented. $\alpha = 12^{\circ}$; $d/c = 0.48$; $V = 140.57$ fps.

Figure 15.- Continued.

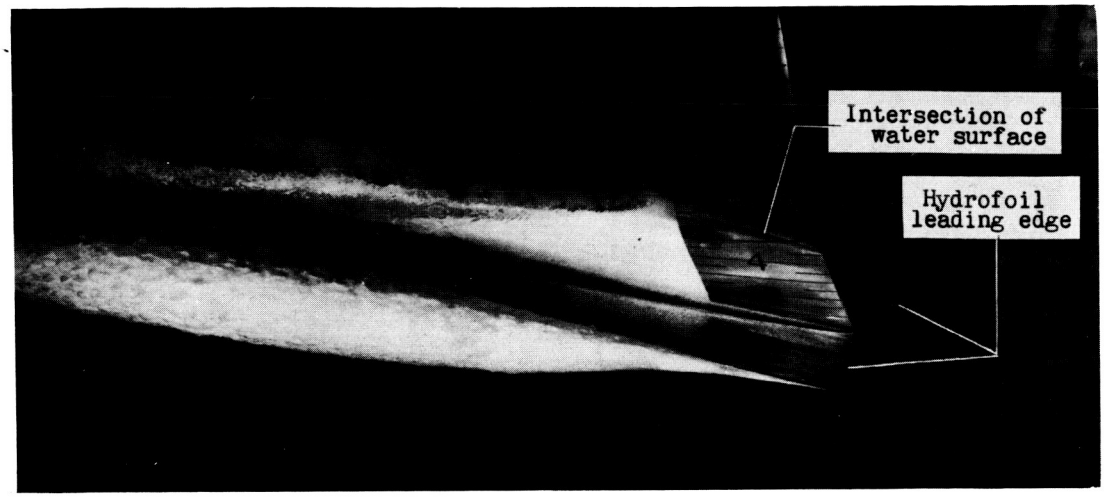

Overhead camera

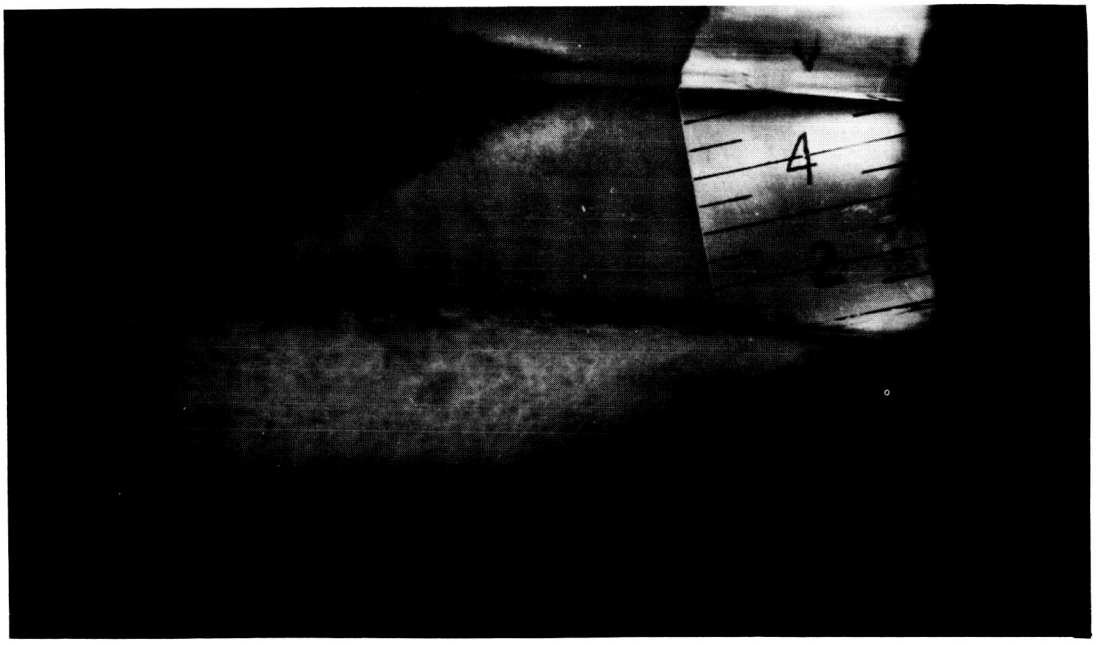

Underwater camera

L-59-6076

(d) Cambered hydrofoil; partially vented. $\alpha = 12^{\circ}$; $d/c = 0.53$; $V = 134.39$ fps.

Figure 15.- Concluded.

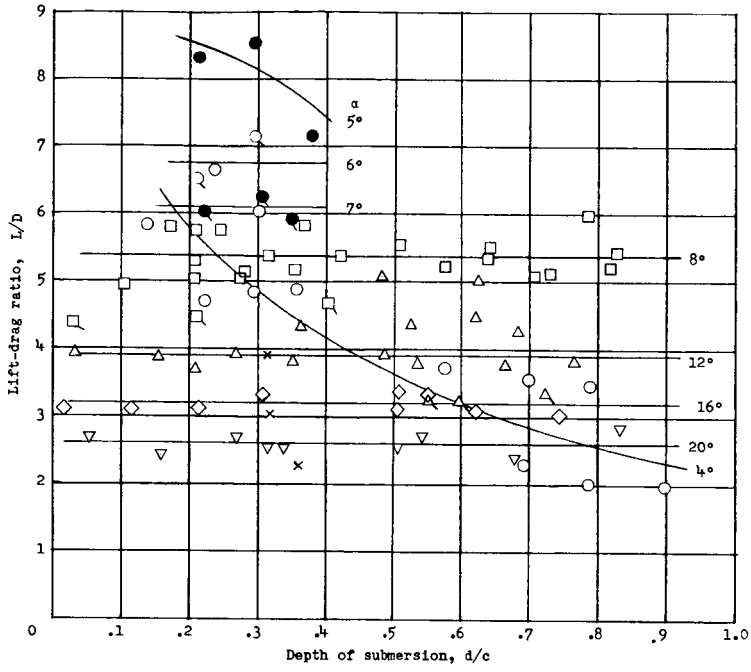

(a) Flat-bottomed hydrofoil.

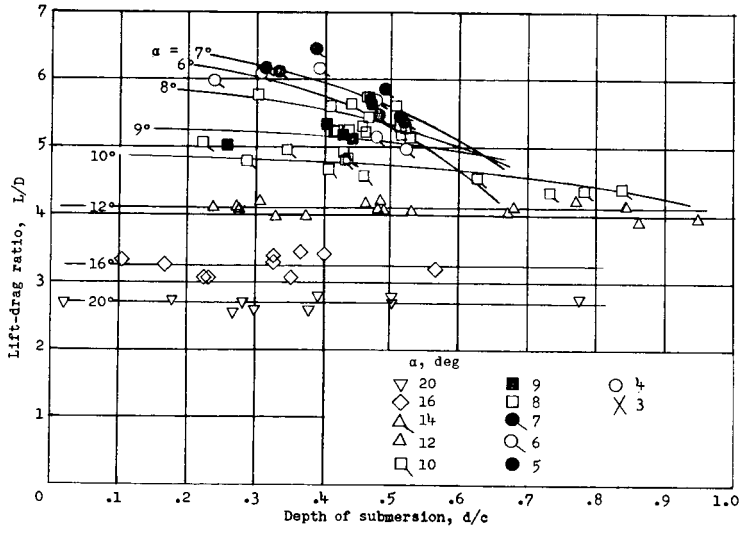

(b) Cambered hydrofoil.

Figure 16.- Variation of lift-drag ratio with depth of submersion for flat-bottomed and cambered hydrofoils at or near zero cavitation number.

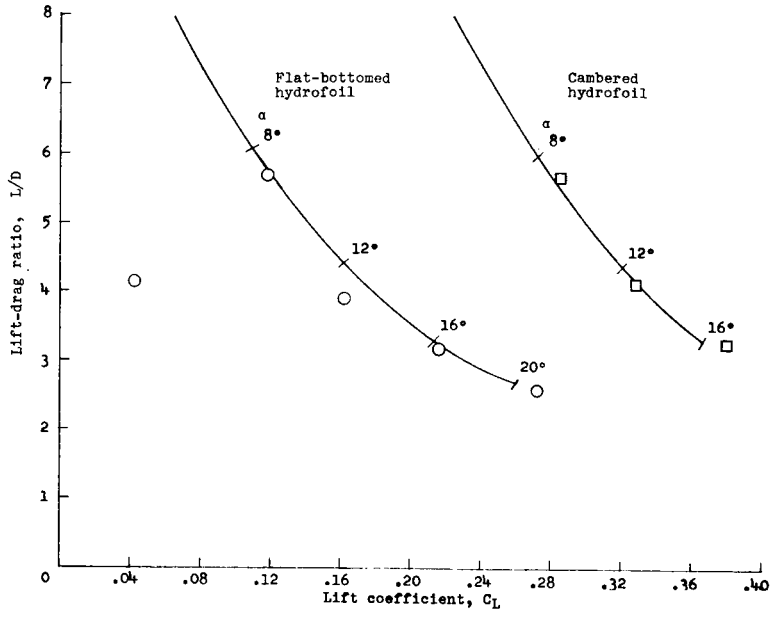

(a) Variation of lift-drag ratio with lift coefficient.

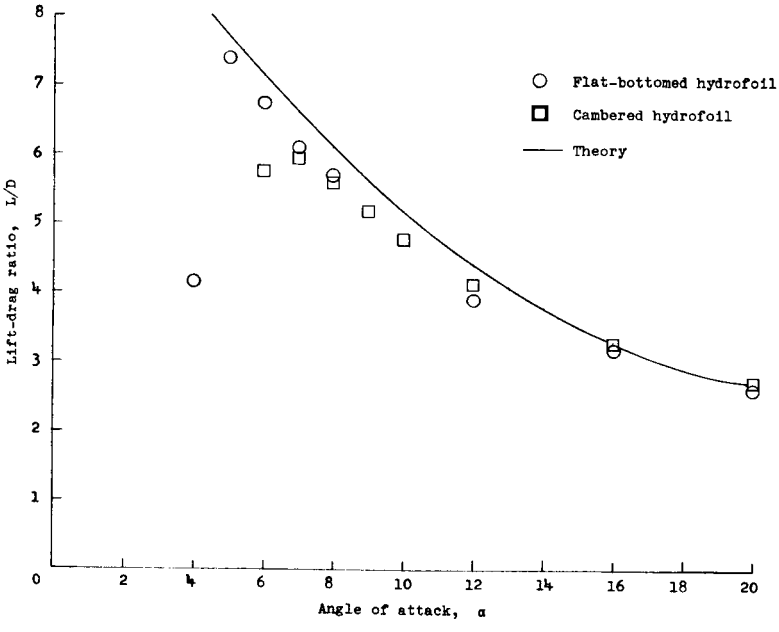

(b) Variation of lift-drag ratio with angle of attack.

Figure 17.- Variation of lift-drag ratio with lift coefficient and angle of attack for flat-bottomed and cambered hydrofoils at d/c = 0.40.

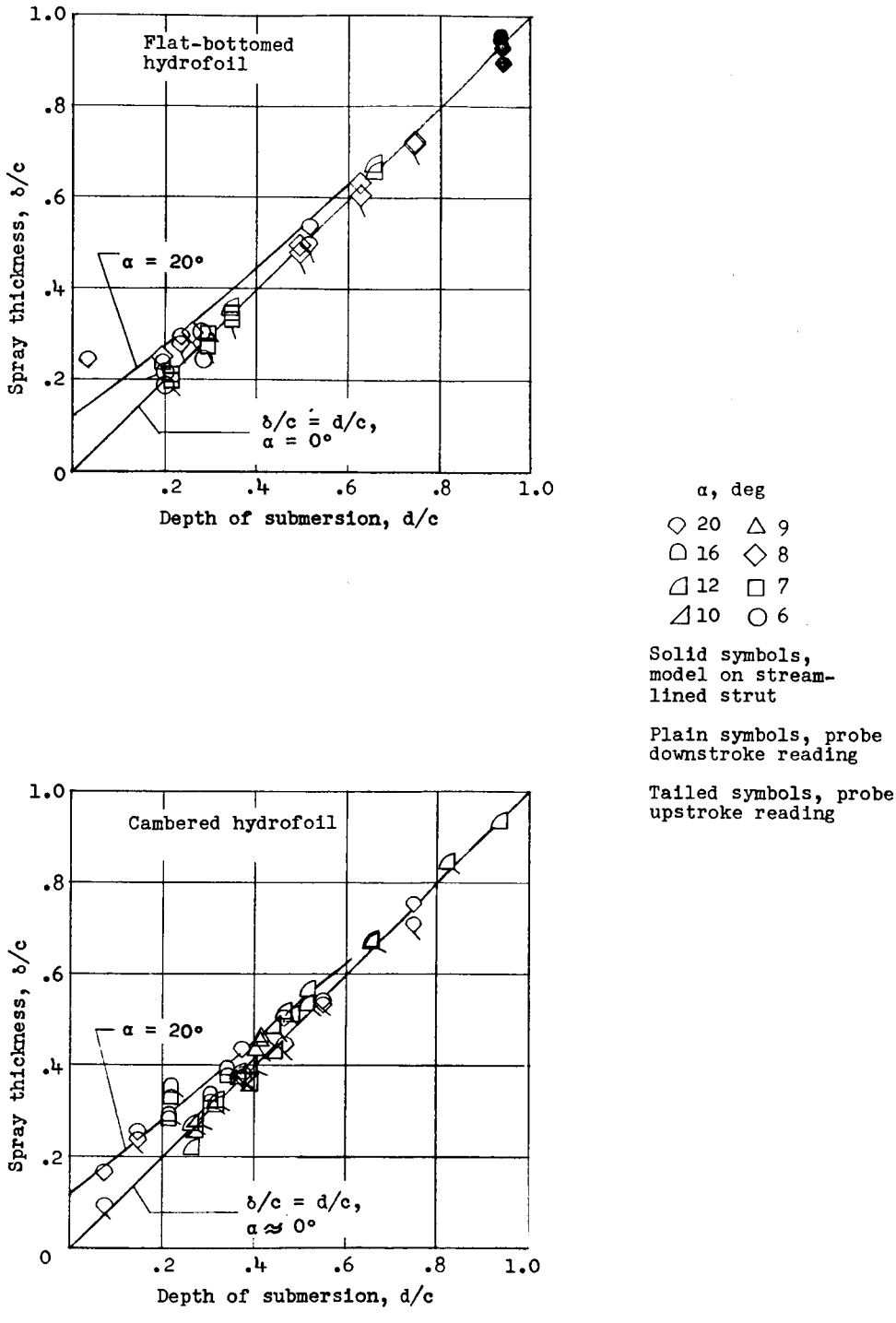

Figure 18.- Variation of spray thickness with depth of submersion for flat-bottomed and cambered hydrofoils.

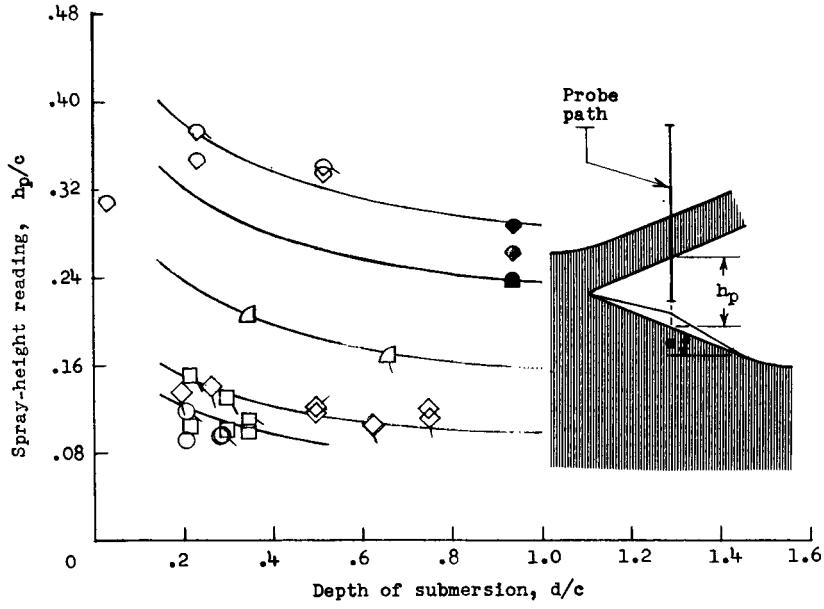

(a) Flat-bottomed hydrofoil.

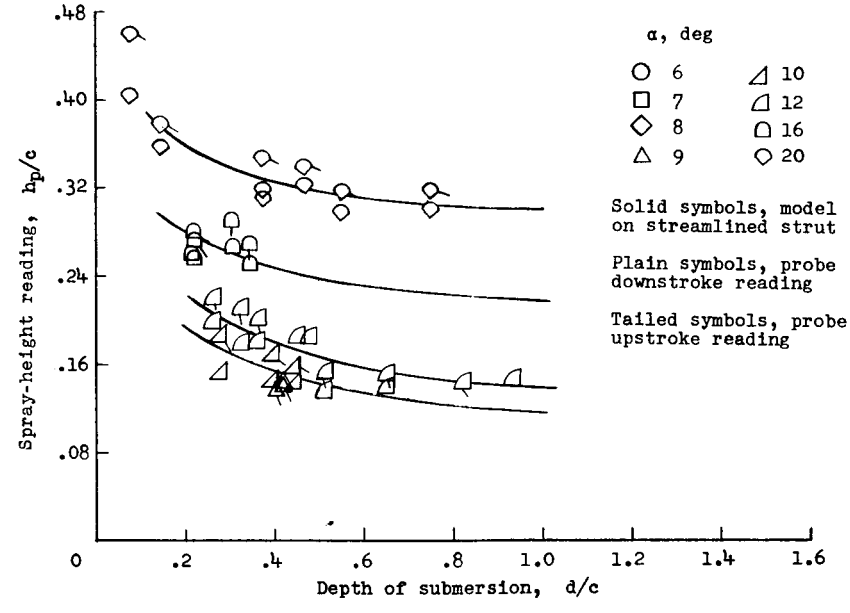

(b) Cambered hydrofoil.

Figure 19.- Variation of spray-height reading with depth of submersion for flat-bottomed and cambered hydrofoils as obtained with probe mechanism.

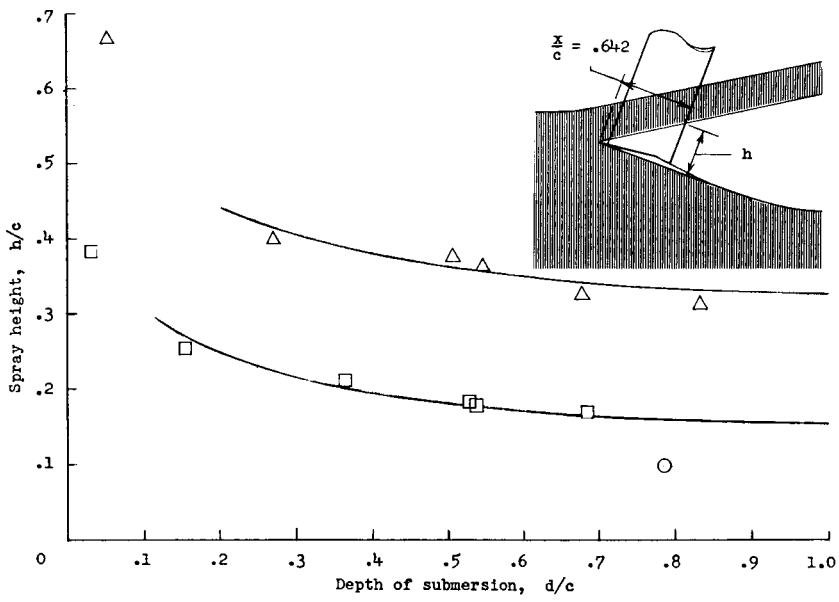

(a) Flat-bottomed hydrofoil.

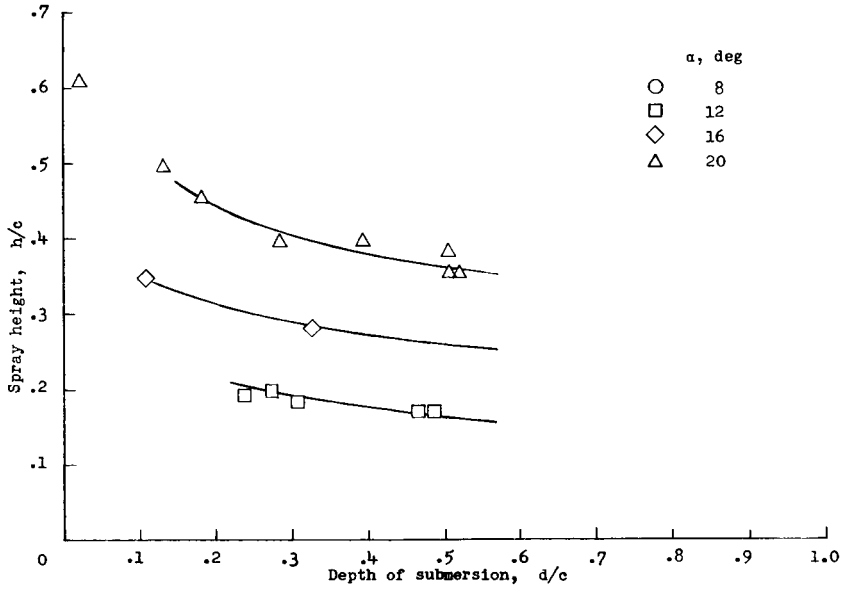

(b) Cambered hydrofoil.

Figure 20.- Variation of spray height above reference line with depth of submersion for flat-bottomed and cambered hydrofoils as read from photographs.

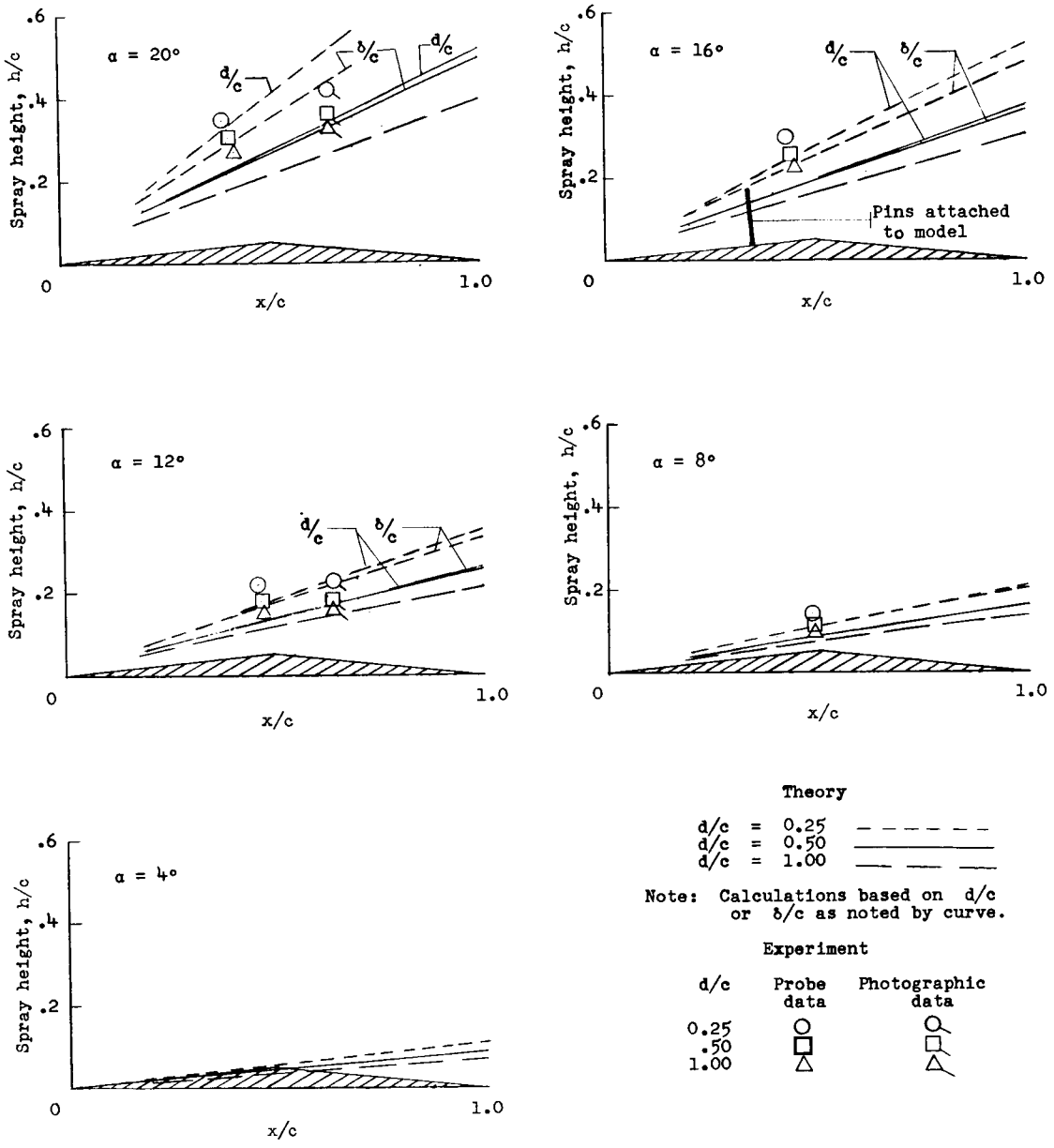

(a) Flat-bottomed hydrofoil.

Figure 21.- Comparison of theoretical spray contours for flat-bottomed and cambered hydrofoils with faired data points obtained with probe mechanism and from photographs.

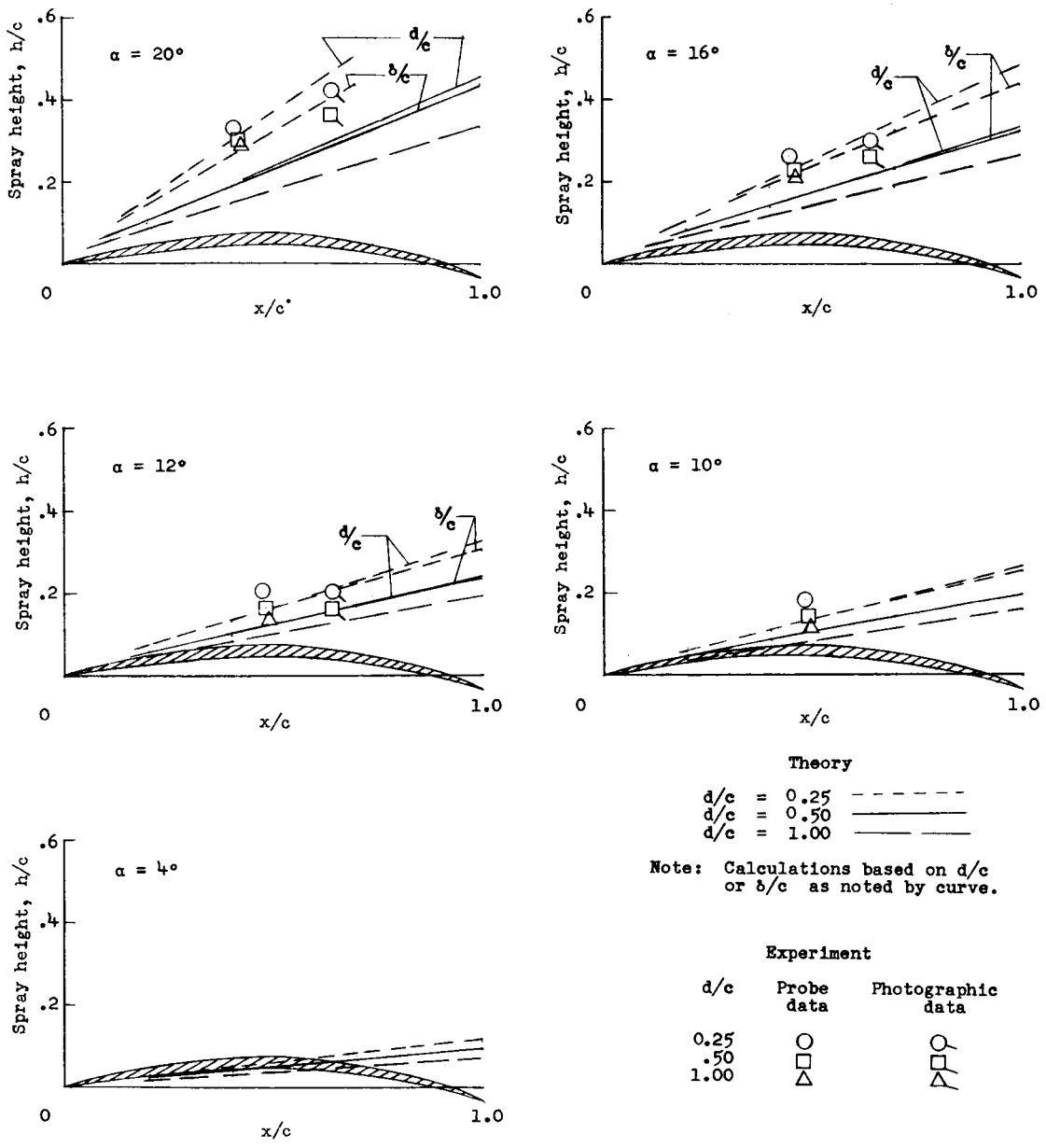

(b) Cambered hydrofoil.

Figure 21.- Concluded.

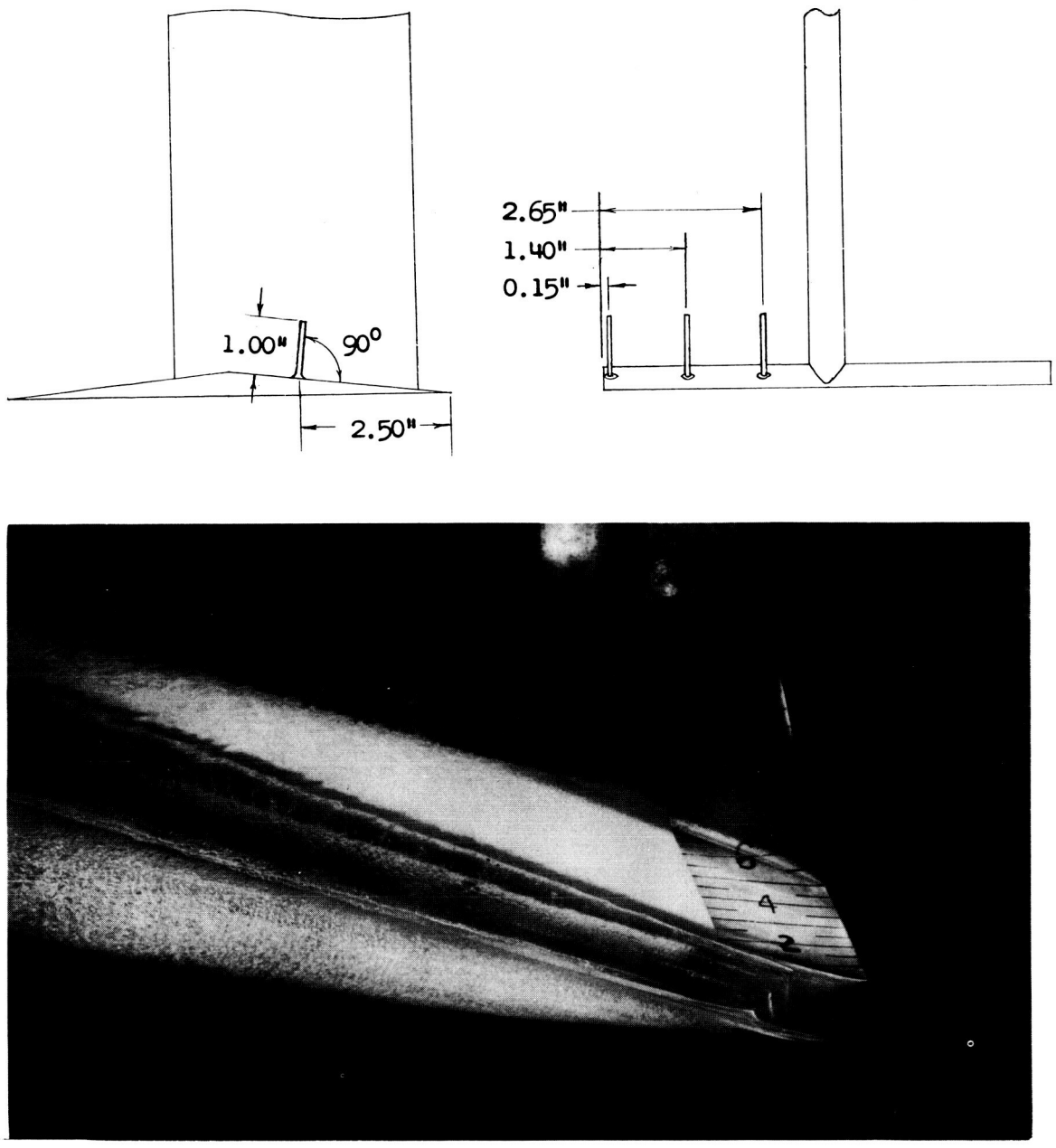

L-59-6077

Figure 22.- Sketch of flat-bottomed hydrofoil with pins attached to upper surface and photograph of flow about hydrofoil with pins attached. $\alpha = 16^{\circ}$; $d/c = 0.51$; $V = 138.05$ fps.

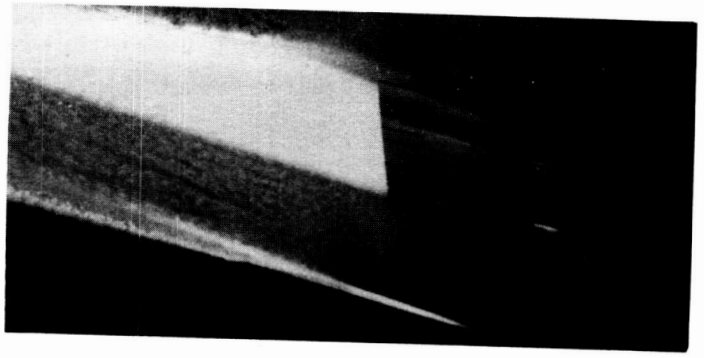

α = 4°; d/c = 0.58; V = 139.22 fps

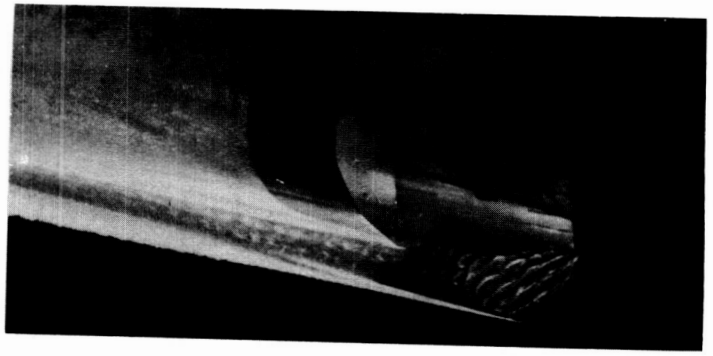

α = 4°; d/c = 0.14; V = 152.19 fps

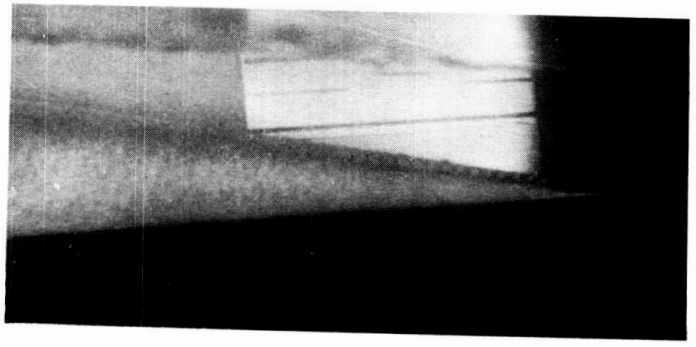

α = 6°; d/c = 0.21; V = 136.77 fps

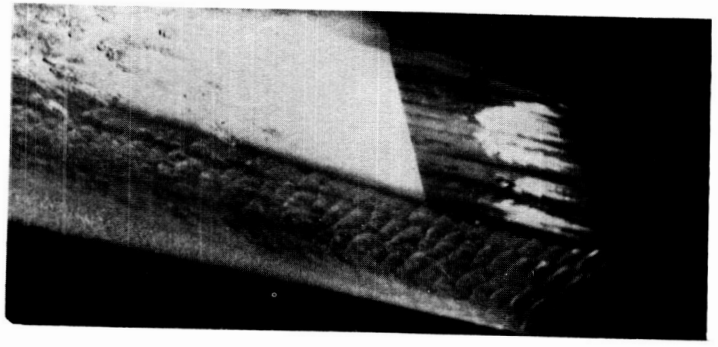

α = 8°; d/c = 0.79; V = 164.50 fps

(a) Flat-bottomed hydrofoil.

L-59-6078

Figure 23.- Photographs of flow about flat-bottomed and cambered hydrofoils at various angles of attack.

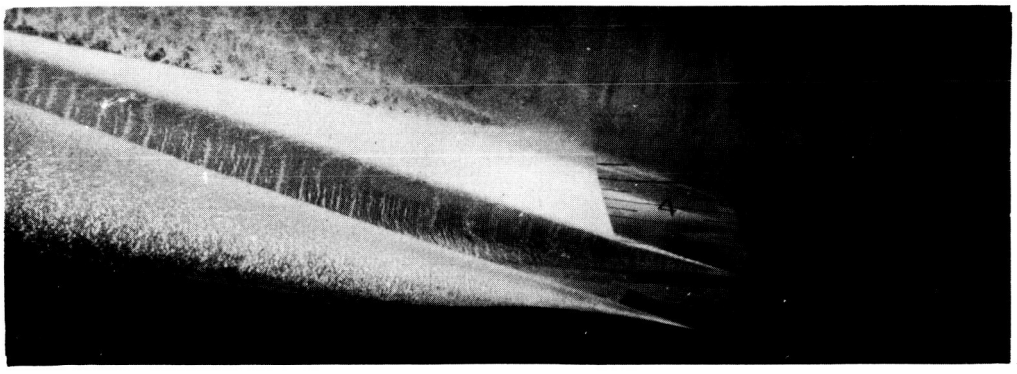

α = 9°; d/c = 0.5 (estimated); V = 145.74 fps

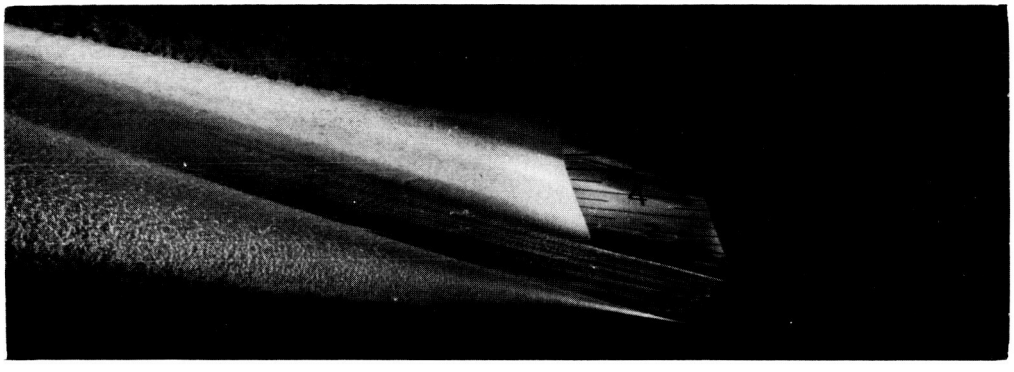

α = 10°; d/c = 0.5 (estimated); V = 139.55 fps

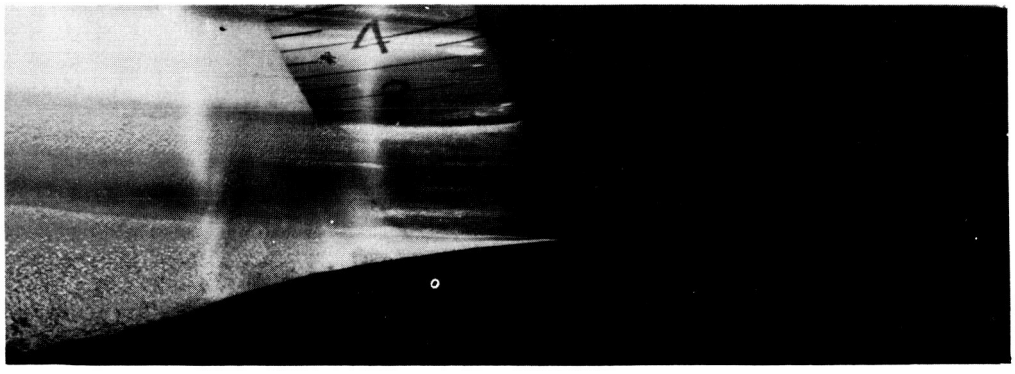

α = 12°; d/c = 0.37; V = 161.34 fps

(b) Cambered hydrofoil. L-59-6079

Figure 23.- Concluded.

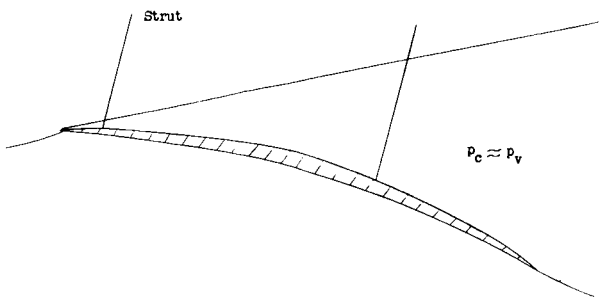

(a) $\sigma = 0$; $V = \infty$.

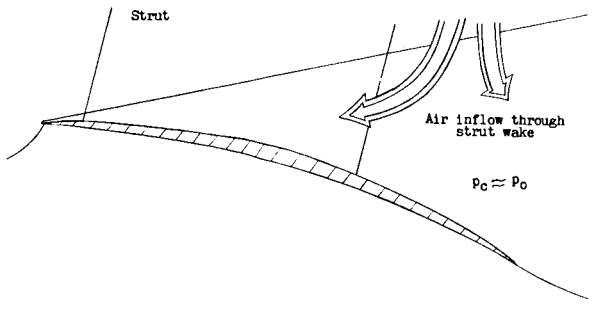

(b) Upper surface unwetted; $\sigma = 0$; $V \neq \infty$.

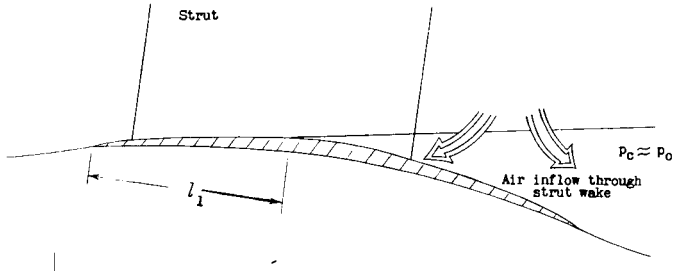

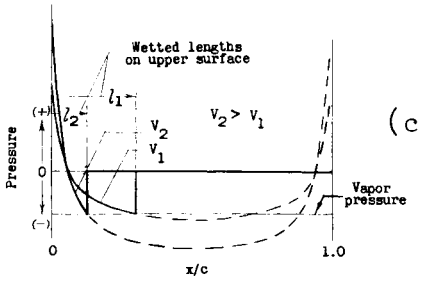

Pressure distribution for part (c)

(c) Upper surface wetted; $\sigma = 0$; $V \neq \infty$.

Figure 24.- Sketches indicating three regimes of flow about cambered hydrofoil at zero cavitation number.

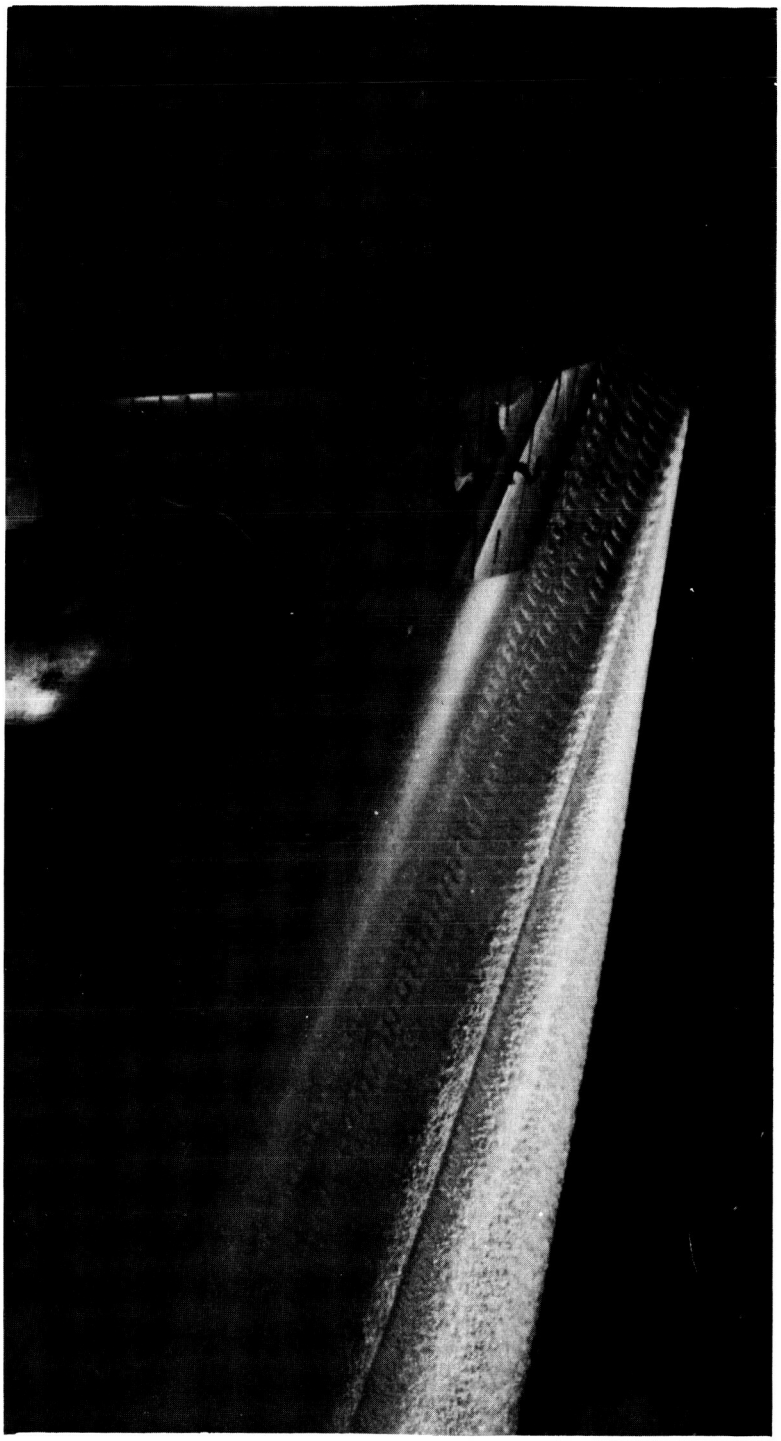

L-59-6080

Figure 25.- Photograph of flow about flat-bottomed hydrofoil indicating leading-edge vibration. $\alpha = 8°$; $d/c = 0.21$; $V = 147.98$ fps.